Available online at www.sciencedirect.com
SCIENCE DIRECT®
Journal of Sound and Vibration 269 (2004) 213–250
JOURNAL OF SOUND AND VIBRATION
www.elsevier.com/locate/jsvi

Energy flow analysis and design sensitivity of structural problems at high frequencies

Nam Ho Kim[a,*], Jun Dong[b], Kyung Kook Choi[b]

[a] *Department of Mechanical and Aerospace Engineering, University of Florida, P.O. Box 116250, Gainesville, FL 32611-6250, USA*

[b] *Center for Computer-Aided Design and Department of Mechanical Engineering, The University of Iowa, Iowa City, IA 52242, USA*

Received 1 February 2002; accepted 14 December 2002

Abstract

The design sensitivity formulation of an energy finite element method is presented using the direct differentiation and adjoint variable methods. The continuum method is used to derive the design sensitivity equation of the energy flow equation, whereas the discrete method is used to calculate the variation of the coupling relation. For design variables, material property, panel thickness, and structural shape are taken into account, in addition to the structural damping factor. The design variable's effect on the power transfer coefficient is discussed in detail. Even if the system matrix equation is not symmetric, the adjoint problem is solved using the same factorized matrix from response analysis. Design sensitivity results calculated from the proposed method are compared to the finite difference sensitivity results with a good agreement.

1. Introduction

Some research has been performed in structural–acoustic design using the finite element method (FEM) and the boundary element method (BEM). Design sensitivity is the most important and expensive information in the modern, gradient-based design optimization process. Ma and Hagiwara [1], Wang et al. [2], Salagame et al. [3], Choi et al. [4], and Scarpa [5] used FEM to calculate the design sensitivity of radiated noise. Kane et al. [6], Smith and Bernhard [7], Cunefare and Koopman [8], Matsumoto et al. [9], Koo [10], and Kim et al. [11] used BEM to calculate the design sensitivity. The continuum method, discrete method, and semi-analytical method are used

*Corresponding author. Tel.: +1-352-846-0665; fax: +1-352-392-7303.
E-mail addresses: nkim@ufl.edu (N.H. Kim), jundong@ccad.uiowa.edu (J. Dong), kkchoi@ccad.uiowa.edu (K.K. Choi).

0022-460X/03/$ - see front matter
doi:10.1016/S0022-460X(03)00070-1

in the calculation of the design sensitivity. However, the practicality of these methods is limited to low-frequency (20–200 Hz) design problems because an excessive number of elements are required in high-frequency analysis [12]. The element size of the structural and acoustic domain must be smaller than the wavelength to ensure an accurate prediction.

Since the response at high frequencies is very sensitive to small changes in the model, statistical energy analysis (SEA) is often used to simulate the structural–acoustic behavior of a large system [13–15]. Given its similarities to the heat transfer problem, this approach uses the conservation of vibration energy within a subsystem of similar modes. From a design point of view, Lu [16] used SEA to find optimum damping factors to control the power flow of a system. However, since single energy value represents the lumped subsystem's status, the energy variation within a subsystem cannot be represented. In addition, the geometric and material parameters, which often serve as design variables, do not appear explicitly in the governing equation.

In contrast to SEA, energy flow analysis (EFA) has been developed using an analytical method that can represent the vibration behavior of a structure in the averaged sense [17–22]. The nearfield response is disregarded in high-frequency ranges, and the farfield response is used to represent the vibration behavior of the structure. Since energy conservation is imposed locally, it is possible to represent the structural geometry in detail, which is critical from a design point of view. Even if the response variable (energy density) is not continuous across structural junctions, this approach has been integrated with FEM to simulate the vibration behavior of a complicated structure at high frequencies [19,23,24].

Although EFA has been applied to engineering applications using the FEM, its design sensitivity analysis and optimization has not been fully developed. Recently, Bitsie and Bernhard [25] differentiate the energy finite element matrix equation with respect to the structural and acoustic damping factors, plate radiation efficiency, and surface sound absorption coefficient. The direct differentiation method and chain rule of differentiation are used to evaluate the sensitivity coefficient of the total energy. Bernhard and Huff [26] studied the effect of panel thickness changes on energy density levels. However, they did not address the computational method to calculate the design sensitivity. For the optimization, Borlase and Vlahopoulos [27] integrated the energy FEM into the design optimization process. The finite difference method (FDM) is used to calculate the design sensitivity coefficient of the energy density with respect to the structural damping factors that are design variables.

In this paper, a rigorous development of design sensitivity analysis for the energy flow problem is presented. The variational equation is differentiated with respect to design variables. Such design variables as material property, panel thickness, and structural shape are taken into account in addition to the structural damping factor. The first two types of design variables refer to a parametric design variable, since the structural configuration does not change during the design process. When the structural shape is a design variable, however, the effect of this variable is complicated, and the concept from the material derivative approach [28] is used in the derivation of the design sensitivity formulation. Two methods are proposed in calculating the design sensitivity: the direct differentiation method and the adjoint variable method. The first method solves for the response variable sensitivity, and the performance sensitivity is then obtained using the chain rule of differentiation. In contrast, the second method computes the performance sensitivity by solving the adjoint problem. Even if the adjoint problem is not symmetric, the

adjoint variable method still uses the same factorized coefficient matrix from response analysis. It is also shown that the adjoint problem is identical for different design variables.

In EFA, the complicated geometry (built-up structures) is assembled from simple structural components (rod, beam, membrane, plate, etc.) by using the power transfer coefficient between components. This power transfer coefficient is a function of the design variables. Thus, in design sensitivity analysis it is necessary to derive the expression of the power transfer coefficient in terms of the design variables. Several methods are proposed to calculate the power transfer coefficient. Langley and Heron [29] proposed an analytical method by using the wave transmission method. De Langhe et al. [30] used finite element analysis and an artificial damping factor that simulates the effect of infinite members. Vlahopoulos et al. [31] proposed an iterative scheme using frequency response analysis. The method of Vlahopoulos et al. [31] is useful when the analytical method cannot be used, such as on a spot-welded structure. In this paper, an analytical method is used to calculate the power transfer coefficient and its sensitivity, because the last two methods present difficulties when used for design sensitivity calculation purposes.

2. Overview of EFA

In order to develop a design sensitivity formulation in the subsequent section, EFA [19–22] and energy finite element analysis [19,23,24] are first reviewed, including a method to calculate the power transfer coefficient.

2.1. Energy flow equation

The energy flow equation for the steady state structural problem can be obtained through the energy conservation relation and the time- and space-averaging process [21] as

$$-\frac{c_g^2}{\eta\omega}\nabla^2 e + \eta\omega e = \pi, \tag{1}$$

where e is the time- and space-averaged energy density function, ∇^2 is the Laplace differential operator, η is the hysteresis-damping factor, ω is the excitation frequency, π is the input power density, and c_g is the group speed [32]. The first term on the left side of Eq. (1) represents the transmitted power, whereas the second term represents the time-averaged dissipated power. Thus, Eq. (1) is the balance between inputted, transmitted, and dissipated powers. Note that the hysteresis-damping factor η is assumed to be small in the derivation of Eq. (1), i.e $\eta \ll 1$.

As discussed by Cho and Bernhard [23], the energy flow equation (1) satisfies within a structural component. Unlike displacement in structural problems, energy density e is not continuous across the junction between structural components. The connection between different components can be achieved through the conservation of power flow and the superposition of vibration energy. Consider a built-up structure made up of a collection of structural components. Each component occupies a domain Ω_i ($\subset R^2$) with boundary Γ_i ($i = 1, \ldots, r$). These domains are interconnected by constraints at each boundary; that is, structural components are connected to adjacent components by junctions that constrain admissible fields.

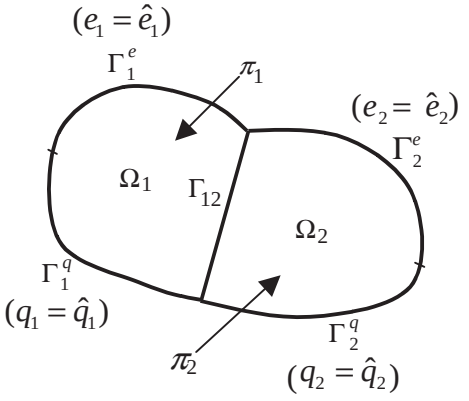

Fig. 1. A built-up structure with components Ω_1 and Ω_2.

Fig. 1 illustrates a simple built-up structure with two components (Ω_1 and Ω_2). The boundary of Ω_i is composed of Γ_i^e, where the energy density e is prescribed, Γ_i^q where the power flow q is prescribed, and the junction boundary Γ_{ij}. In each component Ω_i, the weak formulation of the second order differential equation (1) can be obtained by multiplying the virtual energy density $\bar{e}_i$ with it, and by integrating the equation over the component's domain. After integration by parts, we obtain

$$\int\int_{\Omega_i}\left(\frac{c_{gi}^2}{\eta_i\omega}\nabla\bar{e}_i\cdot\nabla e_i+\eta_i\omega\bar{e}_i e_i\right)\mathrm{d}\Omega=\int\int_{\Omega_i}\bar{e}_i\pi_i\,\mathrm{d}\Omega-\int_{\Gamma_i^e\cup\Gamma_i^q\cup\Gamma_{ij}}\bar{e}_i(\boldsymbol{n}_i\cdot\boldsymbol{I}_i)\,\mathrm{d}\Gamma,\quad i=1,2, \tag{2}$$

where $\nabla e_i=[\partial e_i/\partial x,\partial e_i/\partial y]^{\mathrm{T}}$ is the gradient vector of the energy density, "$\cdot$" is the inner product between vectors and matrices, $\boldsymbol{n}_i$ is the unit outward normal vector to the boundary, and

$$\boldsymbol{I}_i=-\frac{c_{gi}^2}{\eta_i\omega}\nabla e_i, \tag{3}$$

is the time- and space-averaged energy intensity. Since the last integral on the right side of Eq. (2) represents the power flow on the boundary, we can define the relation

$$q_i=\boldsymbol{n}_i\cdot\boldsymbol{I}_i. \tag{4}$$

By using the fact that the virtual energy density $\bar{e}_i$ vanishes on the boundary Γ_i^e, and that the power flow on the boundary Γ_i^q is given, the variational equation of the built-up structure in Fig. 1 can be written as

$$\begin{aligned}\sum_{i=1}^{2}\int\int_{\Omega_i}\left(\frac{c_{gi}^2}{\eta_i\omega}\nabla\bar{e}_i\cdot\nabla e_i+\eta_i\omega\bar{e}_i e_i\right)\mathrm{d}\Omega\\ =\sum_{i=1}^{2}\left(\int\int_{\Omega_i}\bar{e}_i\pi_i\,\mathrm{d}\Omega-\int_{\Gamma_i^q}\bar{e}_i\hat{q}_i\,\mathrm{d}\Gamma\right)-\int_{\Gamma_{12}}(\bar{e}_1 q_1+\bar{e}_2 q_2)\,\mathrm{d}\Gamma,\end{aligned} \tag{5}$$

with the interface condition $q_1+q_2=0$ on Γ_{12}.

In a general setting, let $\boldsymbol{e}$ denote a composite vector of energy density fields in the components making up the built-up structure; that is, $\boldsymbol{e}=[e_1,e_2,\ldots,e_r]^{\mathrm{T}}$, where $e_i\in[H^0(\Omega_i)]^2$ represents the

energy density of the component Ω_i. The space of kinematically admissible fields is defined as a set of energy densities that satisfy homogeneous boundary and interface conditions between components. That is,

$$Z = \{\boldsymbol{e} \in W : \boldsymbol{e} = 0 \text{ on } \Gamma^e \quad \text{and} \quad q_i + q_i = 0 \text{ on } \Gamma_{ij}\}, \tag{6}$$

where the product space $W = \Pi_{i=1}^{r}[H^0(\Omega_i)]^2$ is the space of energy density fields that satisfy the required degree of smoothness, $\Gamma^e = \Gamma_1^e \cup \Gamma_2^e \cup \cdots \cup \Gamma_r^e$ is the essential boundary where the energy density function is prescribed, and Γ_{ij} is the common boundary of components i and j. By using this definition, Eq. (5) satisfies for every $\bar{\boldsymbol{e}} \equiv [\bar{e}_1, \bar{e}_2, \ldots, \bar{e}_r]^{\mathrm{T}}$ belonging to the space Z of kinematically admissible fields.

For convenience in design sensitivity derivations, variational equation (5) can be rewritten using bilinear and linear forms as

$$a_\Omega(\boldsymbol{e}, \bar{\boldsymbol{e}}) + b_\Gamma(\boldsymbol{e}, \bar{\boldsymbol{e}}) = \ell_\Omega(\bar{\boldsymbol{e}}), \quad \forall \bar{\boldsymbol{e}} \in Z, \tag{7}$$

where the bilinear and linear forms are defined as

$$a_\Omega(\boldsymbol{e}, \bar{\boldsymbol{e}}) \equiv \sum_{i=1}^{r} a_{\Omega_i}(e_i, \bar{e}_i) = \sum_{i=1}^{r} \int \int_{\Omega_i} \left(\frac{c_{gi}^2}{\eta_i \omega} \nabla \bar{e}_i \cdot \nabla e_i + \eta_i \omega \bar{e}_i e_i \right) \mathrm{d}\Omega, \tag{8}$$

$$\ell_\Omega(\bar{\boldsymbol{e}}) \equiv \sum_{i=1}^{r} \ell_{\Omega_i}(\bar{e}_i) = \sum_{i=1}^{r} \left[\int \int_{\Omega_i} \bar{e}_i \pi_i \, \mathrm{d}\Omega - \int_{\Gamma_i^q} \bar{e}_i \hat{q}_i \, \mathrm{d}\Gamma \right], \tag{9}$$

$$b_\Gamma(\boldsymbol{e}, \bar{\boldsymbol{e}}) \equiv \sum_{(i,j)=1}^{N_r} b_{\Gamma_{ij}}(e_i, e_j, \bar{e}_i, \bar{e}_j) = \sum_{(i,j)=1}^{N_r} \int_{\Gamma_{ij}} (\bar{e}_j q_i + \bar{e}_i q_j) \, \mathrm{d}\Gamma, \tag{10}$$

where N_r is the number of interfaces within the built-up structure. Note that the bilinear form $a_\Omega(\cdot, \cdot)$ is symmetric with respect to its arguments, while $b_\Gamma(\cdot, \cdot)$ is not. In fact, with its interface condition, $b_\Gamma(\cdot, \cdot)$ represents the conservation of power flow across the discontinuity of the material property or junction geometry.

From a design point of view, the parameters that appear in Eq. (7) can serve as design variables. In the case of a plate-bending problem, for example, the group speed can be written as

$$c_g = 2\sqrt[4]{\frac{\omega^2 D}{\rho h}} = 2\sqrt[4]{\frac{\omega^2 E h^2}{12\rho(1 - v^2)}}, \tag{11}$$

where ρ is the density of the plate, E is Young's modulus, v is the Poisson ratio, h is the thickness of the plate, and D is the flexural rigidity. As will be shown in Section 3, the parameters in Eq. (11), as well as the hysteresis-damping factor η, will serve as parametric design variables. However, in the case of a shape design problem in which the structural domain Ω is itself a design variable, an explicit representation of a design variable as a parameter of the problem is not obvious, which will be discussed in Section 4.

2.2. Finite element discretization

The analytical solution to Eq. (7) can only be obtained for a simple geometry. In general structures, FEM is often used to approximate the solution to Eq. (7). The FEM process involves dividing the structural component's domain Ω_i into a set of simple finite elements Ω_i^m ($m = 1, \ldots, N_i$), and then imposing Eq. (7) on each element. The global system of matrix equations can be obtained through the assembly process. However, the EFA assembly process is different from conventional FEM, because the energy density is not continuous across structural junctions [23]. Instead of the state variable's continuity, the conservation of power flow is used in the assembly process. The structural junction appears when either the material property or the geometric configuration changes. If no junction exists, then a regular finite element assembly process can be used.

In FEM, the energy density in finite element Ω_i^m is approximated using an interpolation vector $\{\boldsymbol{N}_i^m\}$ and a nodal energy density vector $\{\boldsymbol{E}_i^m\}$ as

$$e_i^m = \{\boldsymbol{N}_i^m\}^{\mathrm{T}}\{\boldsymbol{E}_i^m\}. \tag{12}$$

The dimensions $\{\boldsymbol{N}_i^m\}$ and $\{\boldsymbol{E}_i^m\}$ are the same as the number of nodes in element Ω_i^m. Then, the nodal energy density vector of component Ω_i is defined by

$$\{\boldsymbol{E}_i\} = \{\boldsymbol{E}_i^1 \cup \boldsymbol{E}_i^2 \cup \ldots \cup \boldsymbol{E}_i^{N_i}\}^{\mathrm{T}}. \tag{13}$$

The same interpolation method will be used for the virtual energy density $\bar{e}_i$ in the Galerkin approximation. By using the standard Gauss integration method, the bilinear and linear forms in Eqs. (8)–(10) are approximated by

$$\sum_{i=1}^{r} \int\int_{\Omega_i} \left(\frac{c_{gi}^2}{\eta_i \omega} \nabla \bar{e}_i \cdot \nabla e_i + \eta_i \omega \bar{e}_i e_i \right) \mathrm{d}\Omega \approx \sum_{i=1}^{r} \{\bar{\boldsymbol{E}}_i\}^{\mathrm{T}} [\boldsymbol{K}_i] \{\boldsymbol{E}_i\}, \tag{14}$$

$$\sum_{i=1}^{r} \left[\int\int_{\Omega_i} \bar{e}_i \pi_i \, \mathrm{d}\Omega - \int_{\Gamma_i^q} \bar{e}_i \hat{q}_i \, \mathrm{d}\Gamma \right] \approx \sum_{i=1}^{r} \{\bar{\boldsymbol{E}}_i\}^{\mathrm{T}} \{\boldsymbol{F}_i\}, \tag{15}$$

$$\sum_{(i,j)=1}^{N_r} \int_{\Gamma_{ij}} (\bar{e}_i q_i + \bar{e}_j q_j) \, \mathrm{d}\Gamma \approx \sum_{(i,j)=1}^{N_r} \{\bar{\boldsymbol{E}}_i, \bar{\boldsymbol{E}}_j\} \begin{Bmatrix} \boldsymbol{Q}_i \\ \boldsymbol{Q}_j \end{Bmatrix}. \tag{16}$$

The global system of matrix equations can be obtained through the assembly process. After imposing the essential boundary condition, the global system of matrix equations is obtained as

$$[\boldsymbol{K}]\{\boldsymbol{E}\} = \{\boldsymbol{F}\} - \{\boldsymbol{Q}\}, \tag{17}$$

where $\{\boldsymbol{E}\} = \{\boldsymbol{E}_1, \boldsymbol{E}_2, \ldots, \boldsymbol{E}_r\}^{\mathrm{T}}, \{\boldsymbol{F}\} = \{\boldsymbol{F}_1, \boldsymbol{F}_2, \ldots, \boldsymbol{F}_r\}^{\mathrm{T}}, \{\boldsymbol{Q}\} = \{\boldsymbol{Q}_1, \boldsymbol{Q}_2, \ldots, \boldsymbol{Q}_r\}^{\mathrm{T}}$, and

$$[\boldsymbol{K}] = \mathop{\mathsf{A}}_{i=1}^{r} ([\boldsymbol{K}_i]), \tag{18}$$

where A denotes the assembly operator that maps the component's coefficient matrix into the global coefficient matrix.

When discontinuities in the material property and junction shape exist, the power flow vector $\{\boldsymbol{Q}_i\}$ must be calculated from the conservation of power flow across the junction. This process is equivalent to the construction of kinematically admissible fields, defined in Eq. (6). For simplicity,

let the components Ω_i and Ω_j have a single element i and j, respectively, and let elements i and j share the discontinuous junction. Then, the conservation requirement yields the following relation between the power flow and the energy density of two adjacent elements:

$$\begin{Bmatrix} \boldsymbol{Q}_i \\ \boldsymbol{Q}_j \end{Bmatrix} = [\boldsymbol{J}_{ij}] \begin{Bmatrix} \boldsymbol{E}_i \\ \boldsymbol{E}_j \end{Bmatrix}. \tag{19}$$

Note that it is necessary to define duplicate nodes along the junction. Construction of the junction matrix $[\boldsymbol{J}_{ij}]$ involves calculating the power transfer coefficient [23]. Thus, it is critical to calculate the power transfer coefficient in the assembly process. In addition, the power transfer coefficient is a function of the material property, panel thickness, and junction geometry, which are design variables.

Given the relation in Eq. (19), the power flow vector in Eq. (17) moves to the left side of the matrix equation. Thus, the assembled matrix of elements i and j becomes

$$\left[\begin{bmatrix} \boldsymbol{K}_i & \boldsymbol{0} \\ \boldsymbol{0} & \boldsymbol{K}_j \end{bmatrix} + [\boldsymbol{J}_{ij}] \right] \begin{Bmatrix} \boldsymbol{E}_i \\ \boldsymbol{E}_j \end{Bmatrix} = \begin{Bmatrix} \boldsymbol{F}_i \\ \boldsymbol{F}_j \end{Bmatrix}. \tag{20}$$

Due to the asymmetry of the junction matrix $[\boldsymbol{J}_{ij}]$, the coefficient matrix in Eq. (20) is not symmetric. However, it will be shown in the development of the design sensitivity formulation that such asymmetry does not cause any further computational cost in solving the adjoint problem.

2.3. Power transfer matrix

Langley and Heron [29] presented an analytical method for calculating the power transfer coefficient for arbitrary angled plate-to-plate junctions. Such a method is used in this paper for EFA as well as for design sensitivity analysis. The analytical method of calculating power transfer coefficients uses a junction composed of semi-infinite plates. The rationale for applying this semi-infinite theory to the finite-dimension has been discussed by Cremer et al. [32] and Cho [33] through the frequency-averaging process at high frequencies. Consider a set of semi-infinite flat plates connected directly or via a reinforced beam. Given a specific kind of incident wave with unit amplitude on one plate, the amplitudes of the transmitted waves on all coupled plates can be evaluated using the dynamic stiffness matrix method. As a result, based on wave amplitudes the power carried by different waves can be calculated, from which the power transfer coefficient can be obtained. A detailed derivation of the power transfer coefficient is presented in Eq. (A.9) of Appendix A, in conjunction with its sensitivity derivations. In this section, the development of the junction matrix $[\boldsymbol{J}_{ij}]$ in Eq. (19) will be presented.

Consider a junction composed of coupled, co-planar Plates 1 and 2, as shown in Fig. 2. If the plate thicknesses or material properties are different, then the interface between the two plates is defined as a junction. Only a straight-line junction is considered in this paper. Across this junction, the energy density is discontinuous. In Fig. 2, the super-scribed "–" denotes incoming flow, and "+" denotes outgoing flow. For simplicity, only a bending–to–bending vibration is considered. From Fig. 2, the net power flow out of the junction can be written as

$$q_i = q_i^+ - q_i^-, \quad i = 1, 2. \tag{21}$$

The objective is to write the power flow q_i in terms of the energy density.

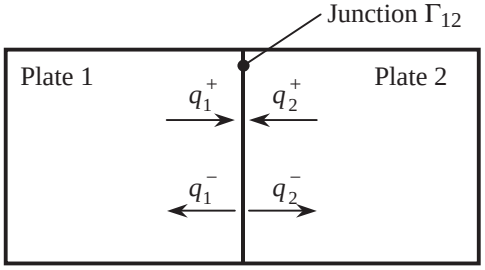

Fig. 2. Power flow at a junction between two co-planar plates.

The incoming power flow to Plate 1 is the summation of the power flow transmitted from Plate 2, plus the power flow reflected at the junction. Let τ_{ij} be the power transfer coefficient (transmission or reflection) from member i to member j. Because of the conservation of power flow across the junction, incoming flows can be expressed using a linear combination of outgoing flows as

$$q_1^- = \tau_{11} q_1^+ + \tau_{21} q_2^+, \quad q_2^- = \tau_{12} q_1^+ + \tau_{22} q_2^+. \tag{22}$$

In addition, the incoming and outgoing power flows can be related with the corresponding energy densities as

$$q_i^+ = c_{gi} e_i^+, \quad q_i^- = c_{gi} e_i^-, \quad i = 1, 2. \tag{23}$$

Thus, by substituting the relation in Eq. (22) into Eq. (21), and by using the relation in Eq. (23), the power flow can be expressed in terms of outgoing energy density as

$$\begin{Bmatrix} q_1 \\ q_2 \end{Bmatrix} = \begin{bmatrix} (1-\tau_{11})c_{g1} & -\tau_{21} c_{g2} \\ -\tau_{12} c_{g1} & (1-\tau_{22})c_{g2} \end{bmatrix} \begin{Bmatrix} e_1^+ \\ e_2^+ \end{Bmatrix} \equiv [\boldsymbol{P}] \begin{Bmatrix} e_1^+ \\ e_2^+ \end{Bmatrix}. \tag{24}$$

Since the energy density is a time- and space-averaged quantity, it is the superposition of the incident and scattered components as

$$e_i = e_i^+ + e_i^-, \quad i = 1, 2. \tag{25}$$

The incoming and outgoing energy densities also have a similar relation as the conservation relation in Eq. (22), namely,

$$\begin{Bmatrix} e_1 \\ e_2 \end{Bmatrix} = \begin{bmatrix} (1+\tau_{11}) & \tau_{21}\alpha \\ \tau_{12}/\alpha & (1+\tau_{22}) \end{bmatrix} \begin{Bmatrix} e_1^+ \\ e_2^+ \end{Bmatrix} \equiv [\boldsymbol{G}] \begin{Bmatrix} e_1^+ \\ e_2^+ \end{Bmatrix}, \tag{26}$$

where $\alpha = c_{g2}/c_{g1}$ is the ratio of the group speeds between two plates. Thus, by substituting the inverse relation of Eq. (26) into Eq. (24), a relation between the power flow and the energy density at the junction is obtained as

$$\begin{Bmatrix} q_1 \\ q_2 \end{Bmatrix} = [\boldsymbol{P}][\boldsymbol{G}^{-1}] \begin{Bmatrix} e_1 \\ e_2 \end{Bmatrix}. \tag{27}$$

This junction relation is used in the assembly process of the global system matrix. Note that the matrices $[\boldsymbol{P}]$ and $[\boldsymbol{G}]$ are functions of the design variables.

From Eq. (16), the power flow vector $\{\boldsymbol{Q}_i\}$ is obtained by integrating the local power flow q_i along the junction Γ_{12} as

$$\left\{ \begin{array}{c} \boldsymbol{Q}_1 \\ \boldsymbol{Q}_2 \end{array} \right\} = \left\{ \begin{array}{c} \int_{\Gamma_{12}} \{\boldsymbol{N}_1\} q_1 \, \mathrm{d}\Gamma \\ \int_{\Gamma_{12}} \{\boldsymbol{N}_2\} q_2 \, \mathrm{d}\Gamma \end{array} \right\} \equiv [\boldsymbol{J}_{12}] \left\{ \begin{array}{c} \boldsymbol{E}_1 \\ \boldsymbol{E}_2 \end{array} \right\}, \tag{28}$$

where $\{\boldsymbol{E}_i\}$ is the $N_p \times 1$ nodal energy density vector of element i, and $[\boldsymbol{J}_{12}]$ is the $2N_p \times 2N_p$ junction matrix. This relation is assembled in the global matrix equation using the local-to-global Boolean operation. Since the interpolation function of those nodes that do not belong to the junction boundary vanishes on Γ_{12}, the size of the junction matrix can be further reduced if such a situation is taken into account.

The junction relation in Eq. (28) corresponds to the simplest situation in the plate-to-plate connection. If two members are met with an arbitrary angle, then the bending, longitudinal, and shear waves must be considered simultaneously. In such a case, the size of the junction matrix becomes $6N_p \times 6N_p$. The junction matrix becomes more complicated when multiple components are connected at the junction. However, the same conservation of power flow can be used, although with algebraic complications.

3. Parameter sensitivity analysis

Design sensitivity is the gradient of a performance measure with respect to design variables. In the structural–acoustic problem, the vibration energy often serves as a performance measure. Parameter sensitivity analysis appears when the parameter of a structural–acoustic problem is a design variable. The thickness of the plate, the material property, the power transfer coefficient, and the hysteresis-damping factor are all examples of parametric design variables.

3.1. Definition of a variation

Let us begin with the definition of a variation that will be frequently used in the following derivations. Throughout this paper, u denotes a parametric design variable. Let ψ be a function that depends on current design u and assume that $\psi(u)$ is continuous with respect to design u. If the current design is perturbed in the direction of δu (arbitrary), and ε is a scalar parameter that controls perturbation size, then the variation of $\psi(u)$ in the direction of δu is defined as

$$\psi'_{\delta u} \equiv \frac{\mathrm{d}}{\mathrm{d}\varepsilon} \psi(u + \varepsilon \delta u) \bigg|_{\varepsilon=0} = \frac{\partial \psi}{\partial u} \delta u. \tag{29}$$

Throughout this paper, the prime symbol "′" is the first variation in the calculus of variations [34]. For convenience, subscribed δu will often be ignored. The term "derivative" or "differentiation" will often be used to denote the variation in Eq. (29), because the coefficient of δu (i.e., $\partial \psi / \partial u$) will be calculated in practice. If the variation of a function is continuous and linear with respect to δu, then the function is differentiable (more precisely, it is Fréchet differentiable). For complicated problems, it is difficult to prove the differentiability of a general function with respect to the design. Such problems will not be investigated in this paper.

Without mathematical proof, the solution $\boldsymbol{e}$ to the energy flow equation in Section 2, given here in the rewritten form

$$a_u(\boldsymbol{e}, \bar{\boldsymbol{e}}) + b_u(\boldsymbol{e}, \bar{\boldsymbol{e}}) = \ell_u(\bar{\boldsymbol{e}}), \quad \forall \bar{\boldsymbol{e}} \in Z, \tag{30}$$

is differentiable with respect to the design. That is, the variation

$$\boldsymbol{e}' = \boldsymbol{e}'(\mathbf{x}; u, \delta u) \equiv \frac{\mathrm{d}}{\mathrm{d}\varepsilon} \boldsymbol{e}(\boldsymbol{x}; u + \varepsilon \delta u)\bigg|_{\varepsilon=0}, \tag{31}$$

exists, and is the first variation of the solution to Eq. (30) at design u and in direction δu of the design change. Note that $\boldsymbol{e}'$ is a function of independent variable $\boldsymbol{x}$, and depends on design u and direction δu. In Eq. (30), the subscribed u is used to emphasize that the bilinear and linear forms depend on design u.

In addition, each of the bilinear and linear forms encountered in Section 2 is assumed differentiable with respect to the design. That is,

$$a'_{\delta u}(\boldsymbol{e}, \bar{\boldsymbol{e}}) \equiv \frac{\mathrm{d}}{\mathrm{d}\varepsilon} a_{u+\varepsilon\delta u}(\tilde{\boldsymbol{e}}, \bar{\boldsymbol{e}})\bigg|_{\varepsilon=0}, \tag{32}$$

$$\ell'_{\delta u}(\bar{\boldsymbol{e}}) \equiv \frac{\mathrm{d}}{\mathrm{d}\varepsilon} \ell_{u+\varepsilon\delta u}(\bar{\boldsymbol{e}})\bigg|_{\varepsilon=0}, \tag{33}$$

$$b'_{\delta u}(\boldsymbol{e}, \bar{\boldsymbol{e}}) \equiv \frac{\mathrm{d}}{\mathrm{d}\varepsilon} b_{u+\varepsilon\delta u}(\tilde{\boldsymbol{e}}, \bar{\boldsymbol{e}})\bigg|_{\varepsilon=0}, \tag{34}$$

exist, where $\tilde{\boldsymbol{e}}$ denotes the state variable $\boldsymbol{e}$, with the dependence on ε being suppressed, and $\bar{\boldsymbol{e}}$ is independent of ε. For example, $a'_{\delta u}(\boldsymbol{e}, \bar{\boldsymbol{e}})$ is the first variation of the bilinear form a_u in the direction of δu. It is assumed that this first variation is continuous and linear in δu; hence, it is the Fréchet derivative of a_u with respect to the design, and as evaluated in the direction of δu. Eqs. (32)–(34) are, in fact, the contributions from the bilinear and linear forms that are explicitly dependent on the design.

3.2. Direct differentiation method

A direct differentiation method calculates the variation of the energy density in Eq. (31) by differentiating Eq. (30) as

$$a_u(\boldsymbol{e}', \bar{\boldsymbol{e}}) + b_u(\boldsymbol{e}', \bar{\boldsymbol{e}}) = \ell'_{\delta u}(\bar{\boldsymbol{e}}) - a'_{\delta u}(\boldsymbol{e}, \bar{\boldsymbol{e}}) - b'_{\delta u}(\boldsymbol{e}, \bar{\boldsymbol{e}}), \quad \forall \bar{\boldsymbol{e}} \in Z. \tag{35}$$

The left side of Eq. (35) presents the terms that are implicitly dependent on the design. Thus, design sensitivity equation (35) solves the implicitly dependent terms by using the explicitly dependent ones. The left side of Eq. (35) is the same as that of Eq. (30) if $\boldsymbol{e}'$ is replaced by $\boldsymbol{e}$. Thus, the design sensitivity equation uses the same coefficient matrix from response analysis with a different load on the right side.

Next, consider a structural–acoustic performance measure that can be written in integral form, as

$$\psi = \int \int_{\Omega} g(\boldsymbol{e}, \nabla \boldsymbol{e}, u + \varepsilon \delta u)\, \mathrm{d}\Omega, \tag{36}$$

where function g is continuously differentiable with respect to its arguments. Functionals in the form of Eq. (36) represent a wide variety of structural–acoustic performance measures. For example, the volume of a structural component can be written with a g that depends explicitly on u; energy intensity can be written in terms of u and $\nabla \boldsymbol{e}$; and energy density at a point can be formally written using the Dirac-δ measure.

To develop the design sensitivity formula, let us take the variation of the functional in Eq. (36), as

$$\psi' = \int \int_{\Omega} (g_{,\boldsymbol{e}} \cdot \boldsymbol{e}' + g_{,\nabla \boldsymbol{e}} \cdot \nabla \boldsymbol{e}' + g_{,u} \delta u) \, \mathrm{d}\Omega. \tag{37}$$

From the definition of function g, it is assumed that the expressions of $g_{,\boldsymbol{e}}$, $g_{,\nabla \boldsymbol{e}}$, and $g_{,u}$ are available. Thus, from the solution $\boldsymbol{e}'$ of design sensitivity equation (35), the variation ψ' can readily be evaluated in the direct differentiation method.

3.3. Adjoint variable method

Recall that $\boldsymbol{e}'$ and $\nabla \boldsymbol{e}'$ depend on the design change direction δu. The objective of the adjoint variable method is to obtain an explicit expression of ψ' in terms of δu, which requires rewriting the first two terms on the right side of Eq. (37) explicitly in terms of δu. For that purpose, an adjoint equation is introduced by replacing $\boldsymbol{e}'$ in Eq. (37) with a virtual energy density $\bar{\boldsymbol{\lambda}} = \{\bar{\lambda}_1, \bar{\lambda}_2, \ldots, \bar{\lambda}_r\}^{\mathrm{T}}$, and by equating the terms involving $\bar{\boldsymbol{\lambda}}$ in Eq. (37) to the bilinear forms in Eq. (30), thus yielding the adjoint equation for the adjoint variable $\boldsymbol{\lambda}$:

$$a_u(\bar{\boldsymbol{\lambda}}, \boldsymbol{\lambda}) + b_u(\bar{\boldsymbol{\lambda}}, \boldsymbol{\lambda}) = \int \int_{\Omega} (g_{,\boldsymbol{e}} \cdot \bar{\boldsymbol{\lambda}} + g_{,\nabla \boldsymbol{e}} \cdot \nabla \bar{\boldsymbol{\lambda}}) \, \mathrm{d}\Omega, \quad \forall \bar{\boldsymbol{\lambda}} \in Z, \tag{38}$$

where the solution $\boldsymbol{\lambda} = \{\lambda_1, \lambda_2, \ldots, \lambda_r\}^{\mathrm{T}}$ is desired, which is the adjoint energy density associated with the performance measure in Eq. (36).

The intention is to express the first two terms on the right side of Eq. (37) in terms of adjoint variable $\boldsymbol{\lambda}$. Since Eq. (38) satisfies for all $\bar{\boldsymbol{\lambda}} \in Z$, Eq. (38) may be evaluated at a specific $\bar{\boldsymbol{\lambda}} = \boldsymbol{e}'$, since $\boldsymbol{e}'$ belongs to space Z. After substitution, we obtain

$$a_u(\boldsymbol{e}', \boldsymbol{\lambda}) + b_u(\boldsymbol{e}', \boldsymbol{\lambda}) = \int \int_{\Omega} (g_{,\mathbf{e}} \cdot \boldsymbol{e}' + g_{,\nabla \boldsymbol{e}} \cdot \nabla \boldsymbol{e}') \, \mathrm{d}\Omega, \tag{39}$$

whose right side is the same as the first two terms of the right side of Eq. (37), which it is now desirable to write explicitly in terms of δu. Similarly, design sensitivity equation (35) may be evaluated at a specific $\bar{\boldsymbol{e}} = \boldsymbol{\lambda}$ to obtain

$$a_u(\boldsymbol{e}', \boldsymbol{\lambda}) + b_u(\boldsymbol{e}', \boldsymbol{\lambda}) = \ell'_{\delta u}(\boldsymbol{\lambda}) - a'_{\delta u}(\boldsymbol{e}, \boldsymbol{\lambda}) - b'_{\delta u}(\boldsymbol{e}, \boldsymbol{\lambda}). \tag{40}$$

The left sides of Eqs. (39) and (40) are equal, thus yielding the following desired relation:

$$\int \int_{\Omega} (g_{,\boldsymbol{e}} \cdot \boldsymbol{e}' + g_{,\nabla \boldsymbol{e}} \cdot \nabla \boldsymbol{e}') \, \mathrm{d}\Omega = \ell'_{\delta u}(\boldsymbol{\lambda}) - a'_{\delta u}(\boldsymbol{e}, \boldsymbol{\lambda}) - b'_{\delta u}(\boldsymbol{e}, \boldsymbol{\lambda}), \tag{41}$$

where the right side is linear in δu and can be evaluated once the state variable $\boldsymbol{e}$ and the adjoint variable $\boldsymbol{\lambda}$ are determined to be the solutions to Eq. (30) and (38), respectively. Substituting the result of Eq. (41) into Eq. (37), the explicit design sensitivity of ψ is obtained as

$$\psi' = \ell'_{\delta u}(\boldsymbol{\lambda}) - a'_{\delta u}(\boldsymbol{e}, \boldsymbol{\lambda}) - b'_{\delta u}(\boldsymbol{e}, \boldsymbol{\lambda}) + \int \int_{\Omega} g_{,u} \delta u \, \mathrm{d}\Omega, \tag{42}$$

where the first three terms on the right depend on the specific problem under investigation.

As was shown in Eq. (35), the direct differentiation method uses the same coefficient matrix as response analysis. However, the format of adjoint equation (38) is different from response analysis because $b_u(\boldsymbol{e}, \bar{\boldsymbol{e}})$ is not symmetric with respect to its arguments. In the early development of the adjoint variable method [28], the symmetric property of the bilinear form plays an important role. However, the definition of the adjoint problem in Eq. (38) does not require the symmetric property of the bilinear form.

3.4. Analytical example: plate component

In this section, explicit expressions of variations in Eqs. (32)–(34) are developed for the plate component, since this component is commonly used in engineering applications. For notational simplicity, expressions in this section correspond to a single component without including the component's index. When a constant input power and a constant power flow are supplied to the structure (see Fig. 3), π and $\hat{q}$ are independent of the parametric design variable, i.e., $\pi' = \hat{q}' = 0$. Thus, from its definition in Eq. (9), the variation of $\ell_u(\bar{e})$ vanishes, i.e., $\ell'_{\delta u}(\bar{e}) = 0$. Since the bilinear form $b_u(e, \bar{e})$ is calculated from the conservation of power flow across a junction, its variation will be calculated along with the finite element discretization in the next section.

The variation of bilinear form $a_u(e, \bar{e})$ depends on the parametric design variable. For derivational convenience, the hysteresis-damping factor is treated separately from other design variables. According to the definition of the variation in Eq. (32), the bilinear form in Eq. (8) is differentiated with respect to η to obtain

$$a'_{\delta\eta}(e, \bar{e}) = \int \int_{\Omega} \left(-\frac{c_g^2}{\eta^2 \omega} \nabla \bar{e} \cdot \nabla e + \omega \bar{e} e \right) \delta\eta \, \mathrm{d}\Omega. \tag{43}$$

For other types of parametric design variables, the dependence of $a_u(e, \bar{e})$ on the design is only through the group speed c_g. Thus, the variation of $a_u(e, \bar{e})$ is obtained by

$$a'_{\delta u}(e, \bar{e}) = \int \int_{\Omega} \left(\frac{2c_g}{\eta \omega} \nabla \bar{e} \cdot \nabla e \right) \delta c_g \, \mathrm{d}\Omega, \tag{44}$$

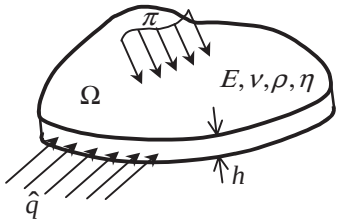

Fig. 3. Parametric design variables of a plate component.

where δc_g is the variation of the group speed. In the case of a bending-to-bending vibration, the expression of δc_g can be obtained from its definition in Eq. (11), which is summarized in Table 1.

Since the result of the structural–acoustic problem is already available, the variation $a'_{\delta u}(e,\bar{e})$ can be readily evaluated for a given δu. In the case of the adjoint variable method, $a'_{\delta u}(e,\lambda)$ is evaluated with the adjoint result λ.

3.5. Finite element discretization

In order to be consistent and efficient, discretization of the design sensitivity equation must follow the same approximation method as the EFA described in Section 2.2. In this section, finite element approximation of the design sensitivity equation is presented using direct differentiation and adjoint variable methods.

3.5.1. Direct differentiation method

The matrices in Eqs. (24) and (26) depend on the design. However, such dependence can only be identified in the discrete form. Accordingly, their sensitivity expressions are developed using the discrete method. By using the fact that the matrices $[\boldsymbol{P}]$ and $[\boldsymbol{G}]$ only have explicitly dependent terms on the design, their variations can be obtained by direct calculation as

$$[\boldsymbol{P}'] = \begin{bmatrix} -\tau'_{11}c_{g1} + (1-\tau_{11})c'_{g1} & -\tau'_{21}c_{g2} - \tau_{21}c'_{g2} \\ -\tau'_{12}c_{g1} - \tau_{12}c'_{g1} & -\tau'_{22}c_{g2} + (1-\tau_{22})c'_{g2} \end{bmatrix}, \tag{45}$$

$$[\boldsymbol{G}'] = \begin{bmatrix} \tau'_{11} & \tau'_{21}\alpha + \tau_{21}\alpha' \\ \tau'_{12}/\alpha - \tau_{12}\alpha'/\alpha^2 & \tau'_{22} \end{bmatrix}, \tag{46}$$

where $\alpha' = c'_{g2}/c'_{g1} - c_{g2}c'_{g1}/c^2_{g1}$, and τ'_{ij} is the variation of the power transfer coefficient, whose expression is presented in Appendix A. By taking the variation of the relation $[\boldsymbol{G}][\boldsymbol{G}^{-1}] = \boldsymbol{I}$, we obtain

$$[\boldsymbol{G}^{-1}]' = -[\boldsymbol{G}^{-1}][\boldsymbol{G}'][\boldsymbol{G}^{-1}]. \tag{47}$$

The dependence of power flow in Eq. (27) is two-fold: the implicit dependence through the energy density e_i and the explicit dependence through the matrices $[\boldsymbol{P}]$ and $[\boldsymbol{G}]$. By using this fact, the variation of the power flow can be obtained by

$$\begin{Bmatrix} q'_1 \\ q'_2 \end{Bmatrix} = [\boldsymbol{P}][\boldsymbol{G}^{-1}] \begin{Bmatrix} e'_1 \\ e'_2 \end{Bmatrix} + ([\boldsymbol{P}'][\boldsymbol{G}^{-1}] + [\boldsymbol{P}][\boldsymbol{G}^{-1}]') \begin{Bmatrix} e_1 \\ e_2 \end{Bmatrix}. \tag{48}$$

Table 1
Variation of the group speed

Design variable	δc_g
H	$(c_g/2h)\delta h$
E	$(c_g/4E)\delta E$
v	$[vc_g/2(1-v^2)]\delta v$
ρ	$-(c_g/4\rho)\delta\rho$

The first term on the right side of Eq. (48) is used to define the junction matrix of the sensitivity equation, while the second term is used to obtain the explicitly dependent term of the power flow vector as

$$b'_{\delta u}(\boldsymbol{e},\bar{\boldsymbol{e}}) = \int_{\Gamma_{12}} \{\boldsymbol{e}\}^{\mathrm{T}}([\boldsymbol{P}'][\boldsymbol{G}^{-1}] + [\boldsymbol{P}][\boldsymbol{G}^{-1}]')\{\boldsymbol{e}\}\,\mathrm{d}\Gamma$$
$$\approx \{\,\bar{\boldsymbol{E}}_1 \quad \bar{\boldsymbol{E}}_2\,\}[\boldsymbol{J}'_{12}]\begin{Bmatrix}\boldsymbol{E}_1\\ \boldsymbol{E}_2\end{Bmatrix}. \tag{49}$$

Discretization of the structural fictitious load in Eq. (32) can be obtained using the energy density $\boldsymbol{e}$. In a plate component, for example, $a'_{\delta u}(\boldsymbol{e},\bar{\boldsymbol{e}})$ in Eq. (44) can be approximated by

$$a'_{\delta u}(\boldsymbol{e},\bar{\boldsymbol{e}}) = \sum_{i=1}^{2}\int\int_{\Omega_i}\left(\frac{2c_{gi}}{\eta_i\omega}\nabla\bar{e}_i\cdot\nabla e_i\right)\delta c_{gi}\,\mathrm{d}\Omega$$
$$\approx \{\,\bar{\boldsymbol{E}}_1 \quad \bar{\boldsymbol{E}}_2\,\}\begin{Bmatrix}\boldsymbol{F}_1^a\\ \boldsymbol{F}_2^a\end{Bmatrix}\delta u, \tag{50}$$

where $\boldsymbol{F}_i^a$ is the nodal fictitious load vector of component i, and δu is the variation of design that appears in Table 1.

Since the left side of sensitivity Eq. (35) is the same as the left side of Eq. (30) by replacing $\boldsymbol{e}'$ with $\boldsymbol{e}$, the approximated sensitivity equation has the same coefficient matrix as in Eq. (20). The global sensitivity matrix equation is obtained from Eqs. (35), (49) and (50), as

$$\left[\begin{bmatrix}\boldsymbol{K}_1 & \boldsymbol{0}\\ \boldsymbol{0} & \boldsymbol{K}_2\end{bmatrix} + [\boldsymbol{J}_{12}]\right]\begin{Bmatrix}\boldsymbol{E}'_1\\ \boldsymbol{E}'_2\end{Bmatrix} = -\begin{Bmatrix}\boldsymbol{F}_1^a\\ \boldsymbol{F}_2^a\end{Bmatrix}\delta u - [\boldsymbol{J}'_{12}]\begin{Bmatrix}\boldsymbol{E}_1\\ \boldsymbol{E}_2\end{Bmatrix}, \tag{51}$$

where the nodal energy density variation $\{\boldsymbol{E}'_i\}$ is solved. After computing $\{\boldsymbol{E}'\} = \{\,\boldsymbol{E}'_1 \quad \boldsymbol{E}'_2\,\}^{\mathrm{T}}$, the variation of energy density is calculated using the same approximation method used in Eq. (12); that is,

$$e'_i = \{\boldsymbol{N}_i\}^{\mathrm{T}}\{\boldsymbol{E}'_i\}, \tag{52}$$

and the sensitivity of the performance measure in Eq. (37) is calculated using the chain rule of differentiation and numerical integration. Since the coefficient matrix of Eq. (51) is factorized during EFA, Eq. (51) can be solved very efficiently.

3.5.2. *Adjoint variable method*

With the adjoint variable method, adjoint variable $\boldsymbol{\lambda}$ is approximated using the same shape function as the energy density function, i.e., $\lambda_i = \{\boldsymbol{N}_i\}^{\mathrm{T}}\{\boldsymbol{\Lambda}_i\}$. The adjoint load, defined in Eq. (38), is calculated using the same finite element approximation method and numerical integration method as

$$\int\int_{\Omega}(g_{,\boldsymbol{e}}\cdot\bar{\boldsymbol{\lambda}} + g_{,\nabla\boldsymbol{e}}\cdot\nabla\bar{\boldsymbol{\lambda}})\,\mathrm{d}\Omega \approx \{\,\bar{\boldsymbol{\Lambda}}_1 \quad \bar{\boldsymbol{\Lambda}}_2\,\}^{\mathrm{T}}\begin{Bmatrix}\boldsymbol{F}_1^{adj}\\ \boldsymbol{F}_2^{adj}\end{Bmatrix}, \tag{53}$$

where $\{\,\bar{\boldsymbol{\Lambda}}_1 \quad \bar{\boldsymbol{\Lambda}}_2\,\}^{\mathrm{T}}$ is the virtual nodal adjoint variable. The adjoint load in the above equation is independent of design variables: it only depends on the performance measure. The left side of

adjoint equation (38) is the transpose of state equation (30) because the bilinear form $b_u(\cdot,\cdot)$ is not symmetric. Thus, the adjoint problem is defined by using the transpose of the coefficient matrix in Eq. (20) as

$$\left[\begin{bmatrix} \boldsymbol{K}_1 & \boldsymbol{0} \\ \boldsymbol{0} & \boldsymbol{K}_2 \end{bmatrix} + [\boldsymbol{J}_{12}]\right]^{\mathrm{T}} \begin{Bmatrix} \boldsymbol{\Lambda}_1 \\ \boldsymbol{\Lambda}_2 \end{Bmatrix} = \begin{Bmatrix} \boldsymbol{F}_1^{adj} \\ \boldsymbol{F}_2^{adj} \end{Bmatrix}. \tag{54}$$

Even if the coefficient matrix in Eq. (54) is the transpose of the coefficient matrix in Eq. (20), the factorized coefficient matrix of Eq. (20) can still be used to solve transposed equation (54). Thus, the computational costs of solving adjoint equation (51) and sensitivity equation (54) are the same.

After solving the adjoint variable $\{\boldsymbol{\lambda}\}$, the performance sensitivity in Eq. (42) is obtained using the numerical integration rule as

$$\psi' = \int\int_{\Omega} g_{,u}\delta u \,\mathrm{d}\Omega - \{\,\boldsymbol{\Lambda}_1 \quad \boldsymbol{\Lambda}_2\,\}\begin{Bmatrix} \boldsymbol{F}_1^a \\ \boldsymbol{F}_2^a \end{Bmatrix}\delta u - \{\,\boldsymbol{\Lambda}_1 \quad \boldsymbol{\Lambda}_2\,\}[\boldsymbol{J}'_{12}]\begin{Bmatrix} \boldsymbol{E}_1 \\ \boldsymbol{E}_2 \end{Bmatrix}. \tag{55}$$

As shown in the above equation, the adjoint variable method still requires the calculation of the fictitious load $\{\boldsymbol{F}^a\}$ and $[\boldsymbol{J}'_{12}]$, which appear in the direct differentiation method. Thus, both methods require the same computational costs, except for the number of matrix equations that need to be solved. The direct differentiation method solves the system of matrix equations according to the number of design variables, while the adjoint variable method solves it according to the number of performance measures.

4. Shape sensitivity analysis

The shape sensitivity formulation is more complicated than parameter sensitivity analysis, since the design variable is the junction angle and the integration domain itself. In this section, the material derivative approach [28] in continuum mechanics is used in the development of shape sensitivity analysis. Even if the shape design variable is different from the parametric design variable, the same form of the adjoint equation as Eq. (38) is obtained for the shape design problem. Only the evaluation stage of the sensitivity coefficient is different for different design variables.

4.1. Material derivatives

The first step in shape sensitivity analysis is to develop relationships between a variation in shape and the resulting variations in functionals. Since the domain shape a structural or acoustic component occupies is treated as the design variable, it is convenient to think of domain Ω as a continuous medium, and to utilize the material derivative idea from continuum mechanics. Due to the design change, a structural or acoustic domain Ω whose boundary is Γ, as shown in Fig. 4, is perturbed to Ω_ε whose boundary is Γ_ε, in which ε is a scalar parameter that controls the amount of perturbation. Only a linear mapping relation will be considered in this paper, such that the

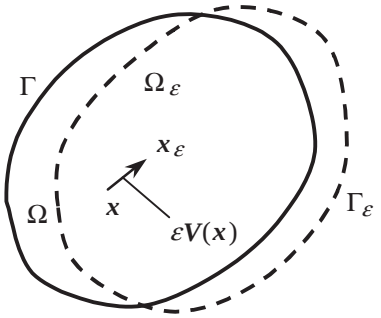

Fig. 4. Variation of domain using linear mapping.

relation between two configurations can be written as

$$\Omega_\varepsilon(\boldsymbol{x};\varepsilon) = \Omega(\boldsymbol{x}) + \varepsilon \boldsymbol{V}(\boldsymbol{x}), \tag{56}$$

where $\boldsymbol{V}(\boldsymbol{x})$ is the design velocity field, which corresponds to the shape design variable. Note that $\Omega_0 = \Omega$. Thus, the shape perturbation in Eq. (56) is similar to the dynamic process, with Ω playing the role of time. If the shape design variable is compared with the parametric design variable, then $\Omega(\boldsymbol{x})$ corresponds to $u(\boldsymbol{x})$, and $\boldsymbol{V}(\boldsymbol{x})$ corresponds to $\delta u(\boldsymbol{x})$.

Using the shape design variable defined in Eq. (56), the material derivative of the solution to the energy flow problem in Eq. (7) can be defined as

$$\dot{\boldsymbol{e}} = \dot{\boldsymbol{e}}(\boldsymbol{x} : \Omega, \boldsymbol{V}) \equiv \frac{\mathrm{d}}{\mathrm{d}\varepsilon}\boldsymbol{e}_\varepsilon(\boldsymbol{x} + \varepsilon \boldsymbol{V}(\boldsymbol{x}))\bigg|_{\varepsilon=0} = \lim_{\varepsilon\to 0}\left[\frac{\boldsymbol{e}_\varepsilon(\boldsymbol{x} + \varepsilon \boldsymbol{V}(\boldsymbol{x}) - \boldsymbol{e}(\boldsymbol{x})}{\varepsilon}\right], \tag{57}$$

where the superposed "dot" denotes the material derivative of the function. The energy density $\boldsymbol{e}$ depends on the shape design variable in two ways. First, its value changes at a fixed point $\boldsymbol{x}$ due to the design change. Second, its value changes due to the perturbation of the material point from $\boldsymbol{x}$ to $\boldsymbol{x} + \varepsilon \boldsymbol{V}$. These two effects can be expressed in mathematical terms as

$$\begin{aligned}\dot{\boldsymbol{e}}(\boldsymbol{x}) &= \lim_{\varepsilon\to 0}\left[\frac{\boldsymbol{e}_\varepsilon(\boldsymbol{x}) - \boldsymbol{e}(\boldsymbol{x})}{\varepsilon}\right] + \lim_{\varepsilon\to 0}\left[\frac{\boldsymbol{e}_\varepsilon(\boldsymbol{x} + \varepsilon \boldsymbol{V}(\boldsymbol{x})) - \boldsymbol{e}_\varepsilon(\boldsymbol{x})}{\varepsilon}\right] \\ &\equiv \boldsymbol{e}'(\boldsymbol{x}) + \nabla \boldsymbol{e} \cdot \boldsymbol{V}(\boldsymbol{x}),\end{aligned} \tag{58}$$

where $\boldsymbol{e}'$ is the partial derivative that is exactly the same as the variation in Eq. (31) for parameter sensitivity analysis, and $\nabla \boldsymbol{e} \cdot \boldsymbol{V}(\boldsymbol{x})$ represents the convective component due to the shape change. The reason for introducing the partial derivative is that it can commute with the gradient operator, i.e., $(\nabla \boldsymbol{e})' = (\nabla \boldsymbol{e}')$. In the case of the material derivative, the following formula must be used:

$$\frac{\mathrm{d}}{\mathrm{d}\varepsilon}\nabla \boldsymbol{e}_\varepsilon\bigg|_{\varepsilon=0} = \nabla \dot{\boldsymbol{e}} - \nabla \boldsymbol{e} \cdot \nabla \boldsymbol{V}. \tag{59}$$

Let ψ_1 be a domain functional, defined as an integral over Ω_ε, namely,

$$\psi_1 = \int\int_{\Omega_\varepsilon} f_\varepsilon(\boldsymbol{x}_\varepsilon)\,\mathrm{d}\Omega_\varepsilon, \tag{60}$$

where f_ε is a regular function defined in Ω_ε. Even if f_ε can be defined at a point, it is more appropriate to define it as an integral form of Eq. (60), in conjunction with the weak formulation

of EFA in Eq. (7). If the domain Ω is smooth, then the material derivative of ψ_1 at Ω is

$$\psi_1' = \int_\Omega [\dot{f}(\boldsymbol{x}) + f(\boldsymbol{x})\text{div } \boldsymbol{V}]\, \mathrm{d}\Omega. \tag{61}$$

The term $\text{div } \boldsymbol{V} = (\partial V_i/\partial x_i)$ represents the effect of domain change. When the Dirac-δ measure is used to define ψ_1 at a point (for example, the energy density at a node), this term vanishes. Note that the notation ψ_1' is used instead of $\dot{\psi}_1$ because in the case of a functional there is no difference between partial and material derivatives.

Although many structural–acoustic functionals can be defined in the form of Eq. (60), there are functionals that are defined as integrals over Γ_ε. For example, the power flow term in Eq. (9) is defined on the natural boundary, and the coupling relation in Eq. (10) is defined on the interface boundary. In the case of a functional ψ_2 that is defined on the boundary,

$$\psi_2 = \int_{\Gamma_\varepsilon} g(\boldsymbol{x}_\varepsilon)\, \mathrm{d}\Gamma_\varepsilon \tag{62}$$

the material derivative of ψ_2 can be obtained from the results of Choi and Haug [28] as

$$\psi_2' = \int_\Gamma [\dot{g}(\boldsymbol{x}) + \kappa g(\boldsymbol{x}) V_n]\, \mathrm{d}\Gamma, \tag{63}$$

where κ is the curvature of the boundary and V_n is the normal component of the design velocity on the boundary. The tangential component of design velocity does not contribute to the shape change. If a constraint is imposed on the design velocity field $\boldsymbol{V}(\boldsymbol{x})$ on the boundary such that it remains straight during design perturbation, then the curvature contribution in Eq. (63) vanishes. The material derivative formulas in Eqs. (61) and (63) will be used to derive the shape design sensitivity equation in the following sections.

4.2. Direct differentiation method

Similar to parameter sensitivity analysis, the direct differentiation method calculates the material derivative $\dot{e}$ by solving the design sensitivity equation, which can be obtained by differentiating Eq. (7) with respect to the shape design variable. For that purpose, let us define the material derivative of those forms that appear in Eq. (7). After separating those terms that contain $\dot{\boldsymbol{e}}$ (implicitly dependent terms) from those that contain $\boldsymbol{V}$ (explicitly dependent terms), the following expressions can be defined:

$$\frac{\mathrm{d}}{\mathrm{d}\varepsilon} a_{\Omega_\varepsilon}(\boldsymbol{e}_\varepsilon, \bar{\boldsymbol{e}})\bigg|_{\varepsilon=0} \equiv a_\Omega(\dot{\boldsymbol{e}}, \bar{\boldsymbol{e}}) + a'_{\boldsymbol{V}}(\boldsymbol{e}, \bar{\boldsymbol{e}}), \tag{64}$$

$$\frac{\mathrm{d}}{\mathrm{d}\varepsilon} \ell_{\Omega_\varepsilon}(\bar{\boldsymbol{e}})\bigg|_{\varepsilon=0} \equiv \ell'_{\boldsymbol{V}}(\bar{\boldsymbol{e}}), \tag{65}$$

$$\frac{\mathrm{d}}{\mathrm{d}\varepsilon} b_{\Gamma_\varepsilon}(\boldsymbol{e}_\varepsilon, \bar{\boldsymbol{e}})\bigg|_{\varepsilon=0} \equiv b_\Gamma(\dot{\boldsymbol{e}}, \bar{\boldsymbol{e}}) + b'_{\boldsymbol{V}}(\boldsymbol{e}, \bar{\boldsymbol{e}}), \tag{66}$$

where $a_\Omega(\dot{\boldsymbol{e}}, \bar{\boldsymbol{e}})$ and $b_\Gamma(\dot{\boldsymbol{e}}, \bar{\boldsymbol{e}})$ are the same as $a_\Omega(\boldsymbol{e}, \bar{\boldsymbol{e}})$ and $b_\Gamma(\boldsymbol{e}, \bar{\boldsymbol{e}})$ in Eq. (7) by replacing $\dot{\boldsymbol{e}}$ with $\boldsymbol{e}$, respectively, and $\bar{\boldsymbol{e}}$ is independent of the shape design variable because it is an arbitrary test function in the space Z. $a'_{\boldsymbol{V}}(\boldsymbol{e}, \bar{\boldsymbol{e}}), \ell'_{\boldsymbol{V}}(\bar{\boldsymbol{e}})$, and $b'_{\boldsymbol{V}}(\boldsymbol{e}, \bar{\boldsymbol{e}})$ represent the terms that are explicitly

dependent on the design velocity $\boldsymbol{V}(\boldsymbol{x})$. If the solution $\boldsymbol{e}$ to the EFA is known, then these terms can be readily calculated. Expressions of these forms will be derived in the analytical example of a specific structural component.

Using the material derivative expressions in Eqs. (64)–(66), a design sensitivity equation is obtained by differentiating the variational equation (7) with respect to the shape design variable. After collecting the implicitly dependent terms on the left side and the explicitly dependent terms on the right, the following design sensitivity equation is obtained:

$$a_\Omega(\dot{\boldsymbol{e}}, \bar{\boldsymbol{e}}) + b_\Gamma(\dot{\boldsymbol{e}}, \bar{\boldsymbol{e}}) = \ell'_{\boldsymbol{V}}(\bar{\boldsymbol{e}}) - a'_{\boldsymbol{V}}(\boldsymbol{e}, \bar{\boldsymbol{e}}) - b'_{\boldsymbol{V}}(\boldsymbol{e}, \bar{\boldsymbol{e}}), \quad \forall \bar{\boldsymbol{e}} \in Z, \tag{67}$$

where the solution $\dot{\boldsymbol{e}}$ is desired. By replacing $\dot{\boldsymbol{e}}$ with $\boldsymbol{e}$, the left side of Eq. (67) is the same as the left side of Eq. (7); the design sensitivity equation uses the same coefficient matrix from EFA with a different power input on the right side.

After calculating $\dot{\boldsymbol{e}}$, the sensitivity of a performance measure that can be written in the following integral form:

$$\psi = \int \int_{\Omega_\varepsilon} g(\boldsymbol{e}_\varepsilon, \nabla \boldsymbol{e}_\varepsilon)\, \mathrm{d}\Omega_\varepsilon \tag{68}$$

can be obtained using the relations in Eqs. (59) and (61) as

$$\begin{aligned} \psi' = & \int \int_\Omega (g_{,\boldsymbol{e}} \cdot \dot{\boldsymbol{e}} + g_{,\nabla \boldsymbol{e}} \cdot \nabla \dot{\boldsymbol{e}})\, \mathrm{d}\Omega \\ & + \int \int_\Omega [g\, \mathrm{div}\, \boldsymbol{V} - g_{,\nabla \boldsymbol{e}} \cdot (\nabla \boldsymbol{e} \cdot \nabla \boldsymbol{V})]\, \mathrm{d}\Omega, \end{aligned} \tag{69}$$

where it is assumed that g is continuously differentiable with respect to its arguments. From the definition of function g, it is also assumed that the expressions of $g_{,\boldsymbol{e}}$ and $g_{,\nabla \boldsymbol{e}}$ are available. Thus, from the design velocity field $\boldsymbol{V}(\boldsymbol{x})$ and from the solution $\dot{\boldsymbol{e}}$ to design sensitivity equation (67), the variation ψ' can be readily evaluated using numerical integration and the chain rule of differentiation.

4.3. Adjoint variable method

Recall that $\dot{\boldsymbol{e}}$ and $\nabla \dot{\boldsymbol{e}}$ implicitly depend on the design velocity field $\boldsymbol{V}(\boldsymbol{x})$. The objective of the adjoint variable method is to obtain an explicit expression of ψ' in terms of $\boldsymbol{V}(\boldsymbol{x})$, which requires rewriting the first integral on the right side of Eq. (69) explicitly in terms of $\boldsymbol{V}(\boldsymbol{x})$. For that purpose, an adjoint equation is introduced by replacing $\dot{\boldsymbol{e}}$ in Eq. (69) with a virtual energy density $\bar{\boldsymbol{\lambda}} = \{\bar{\lambda}_1, \bar{\lambda}_2, \ldots, \bar{\lambda}_r\}^{\mathrm{T}}$, and by equating the terms involving $\bar{\boldsymbol{\lambda}}$ with the bilinear forms in Eq. (7), thus yielding the adjoint equation for the adjoint variable $\boldsymbol{\lambda}$:

$$a_\Omega(\bar{\boldsymbol{\lambda}}, \boldsymbol{\lambda}) + b_\Gamma(\bar{\boldsymbol{\lambda}}, \boldsymbol{\lambda}) = \int \int_\Omega (g_{,\boldsymbol{e}} \cdot \bar{\boldsymbol{\lambda}} + g_{,\nabla \boldsymbol{e}} \cdot \nabla \bar{\boldsymbol{\lambda}})\, \mathrm{d}\Omega, \quad \forall \bar{\boldsymbol{\lambda}} \in Z, \tag{70}$$

where the solution $\boldsymbol{\lambda} = \{\lambda_1, \lambda_2, \ldots, \lambda_r\}^{\mathrm{T}}$ is desired, which is the adjoint energy density associated with the performance measure in Eq. (68). Note that adjoint Eq. (70) of the shape design problem is exactly same as adjoint Eq. (38) of the parametric design problem. Thus, the same adjoint variable can be used for either parametric or shape design problems without any modification.

After following the same procedure described in Eqs. (39)–(41), the first integral on the right side of Eq. (69) is explicitly expressed in terms of the design velocity field as

$$\int\int_{\Omega}(g_{,e}\cdot\dot{\boldsymbol{e}}+g_{,\nabla e}\cdot\nabla\dot{\boldsymbol{e}})\,\mathrm{d}\Omega=\ell'_{\boldsymbol{V}}(\boldsymbol{\lambda})-a'_{\boldsymbol{V}}(\boldsymbol{e},\boldsymbol{\lambda})-b'_{\boldsymbol{V}}(\boldsymbol{e},\boldsymbol{\lambda}),\tag{71}$$

where the right side is linear in $\boldsymbol{V}(\boldsymbol{x})$ and can be evaluated once it is determined that state variable $\boldsymbol{e}$ and adjoint variable $\boldsymbol{\lambda}$ are the solutions to Eqs. (7) and (70), respectively. Substituting the result of Eq. (71) into Eq. (69), the explicit design sensitivity of ψ is obtained as

$$\begin{aligned}\psi'=&\ell'_{\boldsymbol{V}}(\boldsymbol{\lambda})-a'_{\boldsymbol{V}}(\boldsymbol{e},\boldsymbol{\lambda})-b'_{\boldsymbol{V}}(\boldsymbol{e},\boldsymbol{\lambda})\\&+\int\int_{\Omega}[g\,\mathrm{div}\,\boldsymbol{V}-g_{,\nabla e}\cdot(\nabla\boldsymbol{e}\cdot\nabla\boldsymbol{V})]\,\mathrm{d}\Omega,\end{aligned}\tag{72}$$

where the first three terms on the right depend on the specific problem under investigation.

4.4. Analytical example: plate component

In this section, explicit expressions of variations in Eqs. (64)–(66) are developed for the plate component, since this component is commonly used in engineering applications. For notational simplicity, expressions in this section correspond to a single component without inclusion of that component's index.

EFA in Section 2 is based on the flat plate component. A general, curved shell structure must be approximated using plate components with junctions. To satisfy the plane constraint during the design change, the design velocity field must be defined such that the perturbed geometry remains a plane. In such a situation, shape perturbation can be represented by a pure domain change and a rigid-body rotation. Fig. 5 shows a change in shape and a rotation of the flat plate component. The constrained three-dimensional shape change is composed of the in-plane shape change $\boldsymbol{V}(\boldsymbol{x})$ and the out-of-plane rigid-body rotation θ. If a body-fixed local co-ordinate system $C(x_1-x_2-x_3)$

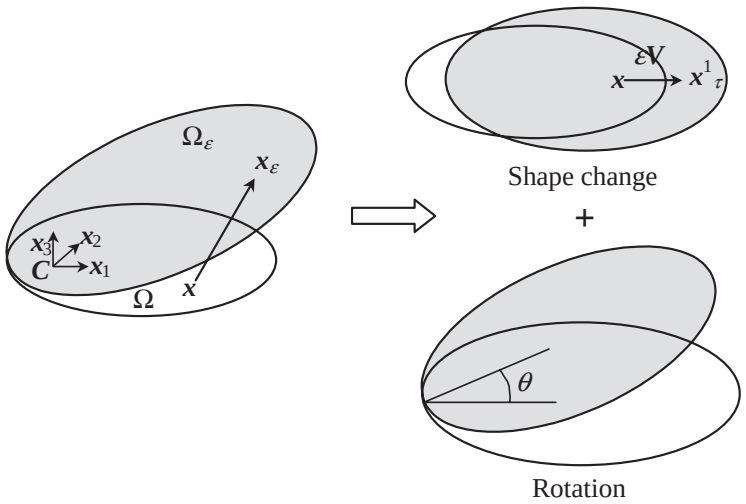

Fig. 5. Perturbation of shape and orientation in surface design component.

is defined with the x_3-axis as normal to the plate, then the in-plane design velocity $\boldsymbol{V}(\boldsymbol{x})$ can be written by the two-dimensional vector $\boldsymbol{V}(\boldsymbol{x}) = \{V_1, V_2, 0\}^{\mathrm{T}}$ in this local co-ordinate system. The shape sensitivity formulations from previous sections can be applied to this two-dimensional design velocity field for the plate component. The rigid-body rotation θ changes the junction angle between components, which is used in the variation of the junction matrix.

The coupling term $b_\Gamma(\boldsymbol{e}, \bar{\boldsymbol{e}})$ is not a function of the component's domain Ω because it is calculated from the junction of semi-infinite plates. It is a function of panel thickness, material property, and junction angle. As was shown in Section 3.5, the explicitly dependent contribution of this coupling term only comes from the power transfer coefficient τ_{ij}. Thus, the expression of $b'_{\boldsymbol{V}}(\boldsymbol{e}, \bar{\boldsymbol{e}})$ in Eq. (66) will be exactly same as $b'_{\delta u}(\boldsymbol{e}, \bar{\boldsymbol{e}})$ if an appropriate τ'_{ij} is used for the junction angle design variable, whose expression is presented in Appendix A.

The variation of the bilinear form $a_\Omega(e, \bar{e})$ and linear form $\ell_\Omega(\bar{e})$ depends on the shape design velocity $\boldsymbol{V}(\boldsymbol{x})$, but not on the rigid-body rotation θ. According to the definition of the material derivative in Eqs. (64) and (65), the explicitly dependent terms of these forms are obtained by using Eqs. (59) and (61), as

$$a'_{\boldsymbol{V}}(e, \bar{e}) = \int\int_\Omega \left(\frac{c_g^2}{\eta\omega} \nabla\bar{e} \cdot \nabla e + \eta\omega \bar{e} e \right) \operatorname{div} \boldsymbol{V} \, \mathrm{d}\Omega - \int\int_\Omega \frac{c_g^2}{\eta\omega} [(\nabla\bar{e} \cdot \nabla \boldsymbol{V}) \cdot \nabla e + \nabla\bar{e} \cdot (\nabla e \cdot \nabla \boldsymbol{V})] \, \mathrm{d}\Omega, \tag{73}$$

$$\ell'_{\boldsymbol{V}}(\bar{e}) = \int\int_\Omega [\bar{e}(\nabla\pi \cdot \boldsymbol{V}) + (\bar{e}\pi) \operatorname{div} \boldsymbol{V}] \, \mathrm{d}\Omega - \int_{\Gamma^q} [\bar{e}(\nabla\hat{q} \cdot \boldsymbol{V}) + \kappa\bar{e}\hat{q}] \, \mathrm{d}\Gamma. \tag{74}$$

As with parameter sensitivity analysis, the partial derivative of the input power and power flow vanishes, i.e., $\pi' = \hat{q}' = 0$. Unlike parameter sensitivity analysis, however, $\ell'_{\boldsymbol{V}}(\bar{e})$ does not vanish because of the shape change. Since the result of the structural–acoustic problem is already available, the variations $a'_{\boldsymbol{V}}(e, \bar{e})$ and $\ell'_{\boldsymbol{V}}(\bar{e})$ can be readily evaluated for a given design velocity $\boldsymbol{V}$. In the case of the adjoint variable method, $a'_{\boldsymbol{V}}(e, \lambda)$ and $\ell'_{\boldsymbol{V}}(\lambda)$ are evaluated with the adjoint result λ.

4.5. Finite element discretization

For a given shape design variable, the discrete design velocity vector $\boldsymbol{V} = \{V_1, V_2\}^{\mathrm{T}}$ and the rigid-body rotation θ must be defined at each node of the finite element. The design velocity within the element is approximated by using the same shape function, as in Eq. (12), while the rotation θ remains constant. As with parameter sensitivity analysis, a simple built-up structure composed of two single-element plate components is considered in the discretization.

4.5.1. Direct differentiation method

If the variation of the power transfer coefficient τ_{ij} is calculated with respect to the design variable θ, then the explicitly dependent term of the power flow vector has the same form as in

Eq. (49). That is,

$$b'_{\boldsymbol{V}}(\boldsymbol{e},\bar{\boldsymbol{e}}) \approx \{\,\bar{\boldsymbol{E}}_1 \quad \bar{\boldsymbol{E}}_2\,\}[\boldsymbol{J}'_{12}]\begin{Bmatrix}\boldsymbol{E}_1\\ \boldsymbol{E}_2\end{Bmatrix}, \tag{75}$$

where $[\boldsymbol{J}'_{12}]$ is calculated from τ'_{ij} with the junction angle θ as the design variable.

The discretization of the fictitious loads in Eqs. (73) and (74) can be obtained using the design velocity $\boldsymbol{V}$ and the energy density $\boldsymbol{e}$. With the plate component, for example, $a'_{\boldsymbol{V}}(\boldsymbol{e},\bar{\boldsymbol{e}})$ and $\ell'_V(\bar{\boldsymbol{e}})$ can be approximated by

$$\begin{aligned} a'_{\boldsymbol{V}}(\boldsymbol{e},\bar{\boldsymbol{e}}) &= \sum_{i=1}^{2}\int\int_{\Omega_i}\frac{c_{gi}^2}{\eta_i\omega}[(\nabla\bar{e}_i\cdot\nabla\boldsymbol{V}_i)\cdot\nabla e_i+\nabla\bar{e}_i\cdot(\nabla e_i\cdot\nabla\boldsymbol{V}_i)]\,\mathrm{d}\Omega\\ &\quad+\sum_{i=1}^{2}\int\int_{\Omega_i}(-\frac{c_{gi}^2}{\eta_i\omega}\nabla\bar{e}_i\cdot\nabla e_i+\eta_i\omega\bar{e}_i e_i)\,\mathrm{div}\,\boldsymbol{V}_i\,\mathrm{d}\Omega\\ &\approx\{\,\bar{\boldsymbol{E}}_1\quad\bar{\boldsymbol{E}}_{\boldsymbol{2}}\,\}\begin{Bmatrix}\boldsymbol{F}_1^a\\ \boldsymbol{F}_2^a\end{Bmatrix}, \end{aligned} \tag{76}$$

$$\begin{aligned} \ell'_{\boldsymbol{V}}(\bar{e}) &= \sum_{i=1}^{2}\int\int_{\Omega_i}[\bar{e}_i(\nabla\pi_i\cdot\boldsymbol{V}_i)+(\bar{e}_i\pi_i)\,\mathrm{div}\,\boldsymbol{V}_i]\,\mathrm{d}\Omega\\ &\quad-\sum_{i=1}^{2}\int_{\Gamma_i^q}[\bar{e}_i(\nabla\hat{q}_i\cdot\boldsymbol{V}_i)+\kappa\bar{e}_i\hat{q}_i]\,\mathrm{d}\Gamma\\ &\approx\{\,\bar{\boldsymbol{E}}_1\quad\bar{\boldsymbol{E}}_2\,\}\begin{Bmatrix}\boldsymbol{F}_1^\ell\\ \boldsymbol{F}_2^\ell\end{Bmatrix}, \end{aligned} \tag{77}$$

where $\boldsymbol{F}_i^\ell-\boldsymbol{F}_i^a$ is the nodal fictitious load vector of component i.

By replacing $\dot{\boldsymbol{e}}$ with $\boldsymbol{e}$, the left side of sensitivity Eq. (67) is the same as the left side of Eq. (7). Thus, the approximated sensitivity equation has the same coefficient matrix as Eq. (20). The global sensitivity matrix equation is obtained from Eqs. (67) and (75)–(77) as

$$\left[\begin{bmatrix}\boldsymbol{K}_1 & \boldsymbol{0}\\ \boldsymbol{0} & \boldsymbol{K}_2\end{bmatrix}+[\boldsymbol{J}_{12}]\right]\begin{Bmatrix}\dot{\boldsymbol{E}}_1\\ \dot{\boldsymbol{E}}_2\end{Bmatrix}=\begin{Bmatrix}\boldsymbol{F}_1^\ell-\boldsymbol{F}_1^a\\ \boldsymbol{F}_2^\ell-\boldsymbol{F}_2^a\end{Bmatrix}-[\boldsymbol{J}'_{12}]\begin{Bmatrix}\boldsymbol{E}_1\\ \boldsymbol{E}_2\end{Bmatrix}, \tag{78}$$

where the nodal energy density variation $\{\dot{\boldsymbol{E}}_i\}$ is desired. After computing $\{\dot{\boldsymbol{E}}\}=\{\,\dot{\boldsymbol{E}}_1\quad\dot{\boldsymbol{E}}_2\,\}^{\mathrm{T}}$, the variation of the energy density is calculated using the same approximation method as in Eq. (12). That is,

$$\dot{e}_i=\{\boldsymbol{N}_i\}^{\mathrm{T}}\{\dot{\boldsymbol{E}}_i\}, \tag{79}$$

and the sensitivity of the performance measure in Eq. (69) is calculated using a chain rule of differentiation and numerical integration. Note that the shape function of the finite element is independent of the shape design variable because it is constructed on the reference geometry.

4.5.2. Adjoint variable method

As was discussed in the previous section, adjoint Eq. (70) for shape sensitivity analysis is the same as adjoint equation (38) for parameter sensitivity analysis. Thus, the same matrix Eq. (54) can be used for shape sensitivity analysis. After solving the adjoint variable $\{\boldsymbol{\lambda}\}$, the performance sensitivity in Eq. (72) is obtained using numerical integration as

$$\psi' = \int\int_{\Omega} [g \operatorname{div} \boldsymbol{V} - g_{,\nabla \boldsymbol{e}} \cdot (\nabla \boldsymbol{e} \cdot \nabla \boldsymbol{V})] \, \mathrm{d}\Omega + \{ \boldsymbol{\Lambda}_1 \quad \boldsymbol{\Lambda}_2 \} \begin{Bmatrix} \boldsymbol{F}_1^{\ell} - \boldsymbol{F}_1^{a} \\ \boldsymbol{F}_2^{\ell} - \boldsymbol{F}_2^{a} \end{Bmatrix} - \{ \boldsymbol{\Lambda}_1 \quad \boldsymbol{\Lambda}_2 \} [\boldsymbol{J}'_{12}] \begin{Bmatrix} \boldsymbol{E}_1 \\ \boldsymbol{E}_2 \end{Bmatrix}. \tag{80}$$

As shown in the above equation, the adjoint variable method still requires the calculation of the fictitious load $\{\boldsymbol{F}^{\ell} - \boldsymbol{F}^{a}\}$ and $[\boldsymbol{J}'_{12}]$, which appear in the direct differentiation method. Thus, these two methods have the same computational cost, except for the number of matrix equations that must be solved.

5. Numerical examples

5.1. Calculation of power transfer coefficients

In order to validate the calculation method of the power transfer coefficient, the same example carried out by Cremer et al. [32] and Langley and Heron [29] is tested. As illustrated in Fig. 6, two semi-infinite plates are connected at a right angle. The same thickness ($h = 1.0\,\mathrm{mm}$) and material properties ($E = 209\,\mathrm{GPa}$, $\nu = 0.3$, $\rho = 7,800\,\mathrm{kg/m^3}$) are used for both plates. An incident bending wave with a frequency of $\omega = 26.687\,\mathrm{kHz}$ is considered. Since the plates are not co-planar, three different types of waves are taken into account: "L" for the longitudinal wave, "S" for the shear wave, and "B" for the bending wave. Thus, τ_{11}^{BL} is the power ratio between the incident bending wave and the reflected longitudinal wave, while τ_{12}^{BS} is the power ratio between the incident

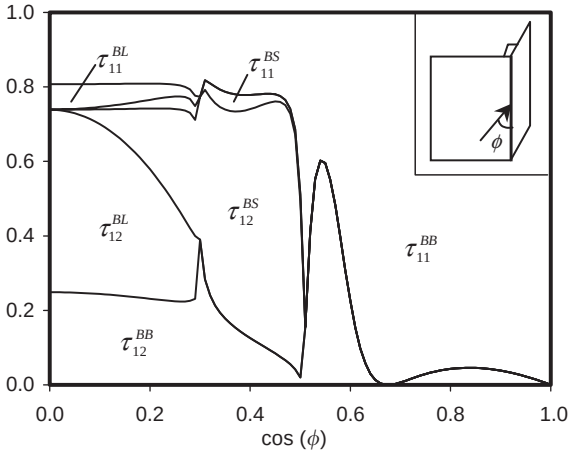

Fig. 6. Power transfer coefficients between two plates connected at a right angle ($h = 1.0\,\mathrm{mm}$, $\omega = 26.687\,\mathrm{kHz}$).

bending wave and the transferred shear wave. The power transfer coefficients at a junction are plotted as a function of the incident wave angle, as shown in Fig. 6, which agree with the results of Cremer et al. [32], and Langley and Heron [29]. The area corresponding to each power transfer coefficient must be integrated throughout the incident angle in order to calculate the power transfer coefficient at the junction.

5.2. Parametric study of design variables

5.2.1. Two co-planar plates

In order to control power flow between structural members, it is necessary to control the power transfer coefficient. Since the power transfer coefficient is the ratio between incident and transmitted powers, a panel thickness change will affect the power transfer coefficient. Fig. 7 shows two co-planar plates with the same material properties ($E = 209\,\text{GPa}$, $v = 0.3$, $\rho = 7,800\,\text{kg/m}^3$). An incident wave with a frequency of $\omega = 2.0\,\text{kHz}$ is considered. The thickness of Plate 1 changes from 0.5 to 1.5 mm, while the thickness of Plate 2 is fixed at 1.0 mm. Only bending-to-bending power transmission is considered, because the plates are co-planar. When the thickness of the two plates is the same (1.0 mm), the power transfer coefficients τ_{12}^{BB} and τ_{21}^{BB} between Plates 1 and 2 become one, which means that energy density is continuous across the junction. As the thickness begins to differ between the two plates, the values of the power transfer coefficients change from one. The maximum change occurs when the thickness of Plate 1 is 0.5 mm, and the value of τ_{12}^{BB} is reduced to 70%.

To investigate further the effect of structural design variables on the power transfer coefficient, variations of energy density as a function of panel thickness are studied for the co-planar plates, as shown in Fig. 8. Unit power density ($\text{J/m}^2\,\text{s}$) is applied at the center of Plate 1. In Fig. 7, point 1 corresponds to the center of Plate 1, and point 2 corresponds to the center of Plate 2. The hysteresis-damping factor of $\eta = 0.01$ is used for both plates. Initially, two plates have the same thickness of 1.0 mm. The energy densities at the center point of these plates are plotted by changing the thickness of the left plate from 0.5 to 1.5 mm. By reducing the thickness of the left plate by 0.5 mm, its energy density at the center increases by 30%, while the energy density at the

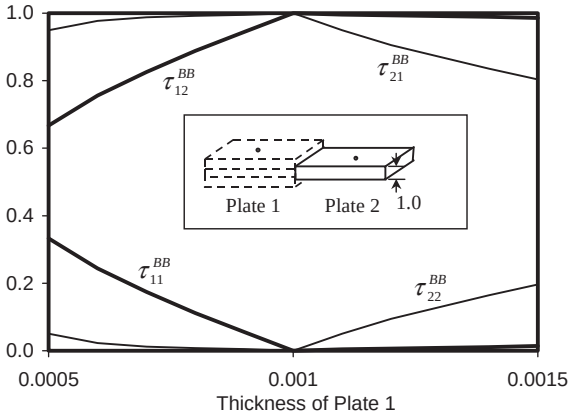

Fig. 7. Variations of the power transfer coefficients as a function of panel thickness.

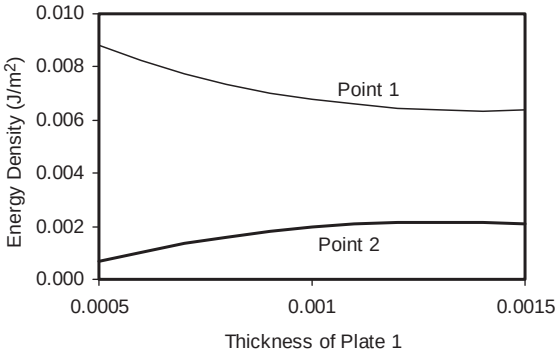

Fig. 8. Variations of the energy densities as a function of a panel thickness.

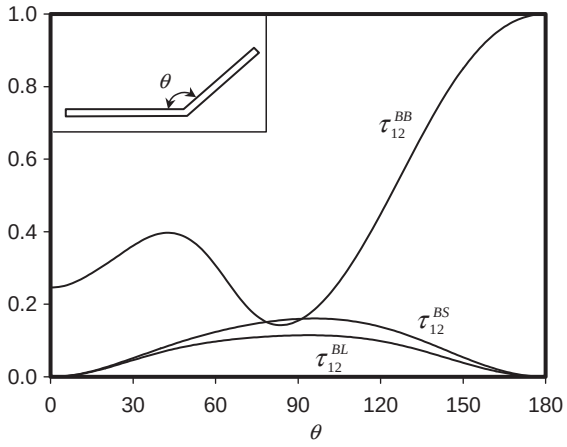

Fig. 9. Variations of the power transfer coefficients as a function of the junction angle.

center of the right plate decreases by 64%. Thus, in this simple example, the ratio of the energy density change appears to be greater than the ratio of the design variable change.

Although the differentiability of the energy density with respect to the design is not proved in the theoretical sections of this study, the power transfer coefficient in Fig. 7 and the energy density in Fig. 8 show smooth variations of the energy density as a function of the thickness design variable.

5.2.2. *Two angled plates*

A change in the power transfer coefficient is more significant if the junction angle between two plates is the design variable, because an incident wave will be transferred to different types of waves. Fig. 9 charts the variation of the power transfer coefficient as a function of the junction angle. The same thickness ($h = 1.0\,\text{mm}$) and material properties ($E = 209\,\text{GPa}$, $\nu = 0.3$, $\rho = 7,800\,\text{kg/m}^3$) are used for both plates. An incident wave with a frequency of $\omega = 26.687\,\text{kHz}$ kHz is considered. The results in Fig. 9 are in good agreement with the results of Langley and Heron [29]. Even if the incident wave is assumed to be a bending wave, three wave types (bending,

longitudinal and shear) are generated because the junction is not co-planar. However, it is clear that when the junction angle is 0° or 180°, those two in-plane power transfer coefficients vanish. As expected, the bending-to-bending power transfer coefficient becomes 1.0 when the plates are co-planar (180°). In addition, the effect of the bending-to-bending power transfer coefficient is dominant for an obtuse angle. As the junction angle changes from 84° to 180°, the bending-to-bending power transfer coefficient increases about seven times. Thus, the junction angle design variable has a significant effect on the power flow between structural members.

5.3. Sensitivity analysis of power transfer coefficients

5.3.1. Parameter design sensitivity (panel thickness)

The parametric study in Section 5.2 shows that the power transfer coefficients depend on design variables. For example, Fig. 10 plots the variations of a bending-to-bending power transfer coefficient as a function of thickness design variables. Two semi-infinite plates are connected at a right angle. The thickness of Plate 1 (incident plate) is fixed at 1.0 mm, while the thickness of Plate 2 varies from 0.5 to 1.5 mm. The same material properties ($E = 209\,\text{GPa}$, $\nu = 0.3$, $\rho = 7,800\,\text{kg/m}^3$) are used for both plates. An incident wave with a frequency of $\omega = 2.0\,\text{kHz}$ is considered. Different from the co-planar plates in Fig. 7, the reflection power transfer coefficient τ_{11}^{BB} is greater than the transferred power transfer coefficient τ_{12}^{BB}. In addition, the summation of τ_{11}^{BB} and τ_{12}^{BB} is not one because the bending incident wave is transmitted as bending, in-plane, and shear wave, although the bending-to-bending transmission is the dominant mode. The sensitivity of these power transfer coefficients with respect to plate thickness is represented by the slope of the curves in Fig. 10.

The analytical sensitivity of the power transfer coefficient is found by differentiating the procedure for calculating the power transfer coefficient, as briefly summarized in Appendix A. In order to verify the accuracy of the results calculated from the formula in Appendix A, Fig. 11 compares the analytical sensitivity results of the power transfer coefficients with the sensitivity results calculated using the FDM. The finite difference sensitivity of τ_{11}^{BB}, for example, can be

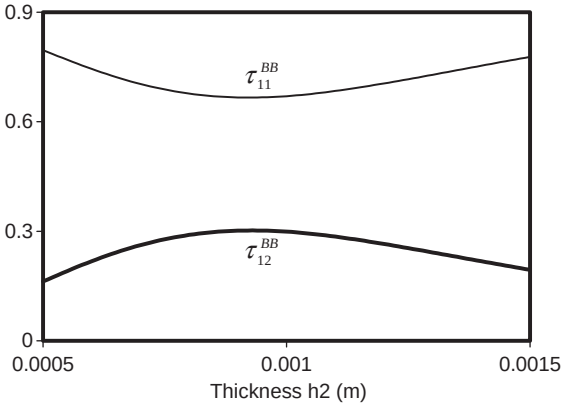

Fig. 10. Variation of the power transfer coefficient as a function of the plate thickness design ($\omega = 2.0\,\text{kHz}$).

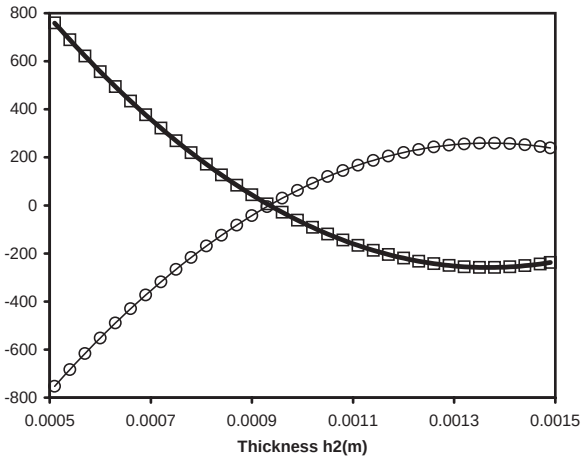

Fig. 11. Sensitivity results of power transfer coefficients compared with the finite difference results for the plate thickness design ($\omega = 2.0$ kHz): ○, $\tau_{11}^{BB'}$ FDM; ——, $\tau_{11}^{BB'}$ analytical; □, $\tau_{12}^{BB'}$ FDM; ——, $\tau_{12}^{BB'}$ analytical.

calculated from

$$\tau_{11}^{BB'}(h) \approx \frac{\tau_{11}^{BB}(h + \Delta h) - \tau_{11}^{BB}(h)}{\Delta h}, \tag{81}$$

where $\Delta h = 0.01$ mm is used. The sensitivity $\tau_{11}^{BB'}$ from Eq. (81) is usually more accurate as perturbation size Δh decreases. However, numerical noise becomes dominant if Δh is so small that the change of τ_{11}^{BB} becomes smaller than the machine's significant digit. Thus, it is always difficult to select the appropriate perturbation size in FDM. In Fig. 11, "$\tau_{11}^{BB'}$ FDM" represents the sensitivity of τ_{11}^{BB} calculated using the FDM, while "$\tau_{11}^{BB'}$ Analytical" represents the sensitivity of τ_{11}^{BB} calculated from the proposed continuum sensitivity formula in Section 3. As shown in Fig. 11, the analytical sensitivity results agree with the finite difference sensitivity results.

5.3.2. Shape design sensitivity (junction angle)

The shape design variable in the plate-based built-up structure can be categorized by the change in the structural domain and the junction angle. Since the power transfer coefficient is calculated based on the connection between semi-infinite plates, the change in the structural domain is not involved. Thus, in this section the junction angle design variable is taken into account to calculate the sensitivity of the power transfer coefficient.

The same semi-infinite plates from Section 5.3.1 are used to validate the sensitivity results when the junction angle is a design variable. The thickness of the two plates is fixed at 1.0 mm, and the junction angle changes from 0° to 180°, as plotted in Fig. 12. Although it is impossible to connect two plates at an angle of 0°, this angle is plotted to be mathematically complete. As expected, τ_{11}^{BB} vanishes when the junction angle becomes 180° because no discontinuity exists; no bending energy will be reflected from the junction. The bending-to-bending power transfer coefficients change rapidly near the junction angles 0° and 180°, while changing slowly between 40° and 140°. Thus, the effect of junction angle design is significant when two plates are connected in a co-planar rather than an orthogonal way. Again, the analytical sensitivity results agree with the finite difference sensitivity results, as shown in Fig. 13. A small design perturbation of $\Delta\theta = 1°$ is used with the FDM.

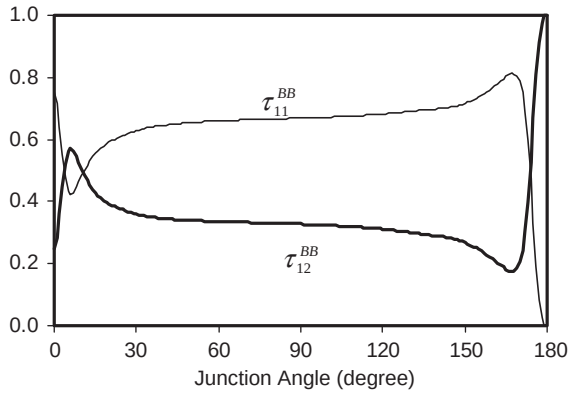

Fig. 12. Variation of the power transfer coefficient as a function of the junction angle design ($\omega = 2.0\,\text{kHz}$).

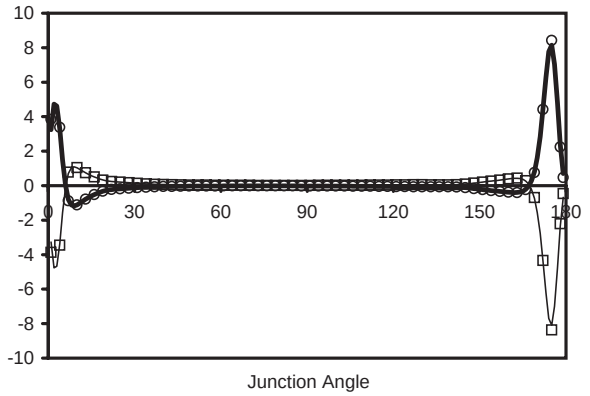

Fig. 13. Sensitivity results of power transfer coefficients compared with the finite difference results for the junction angle design ($\omega = 2.0\,\text{kHz}$): □, $\tau_{11}^{BB'}$ FDM; ——, $\tau_{11}^{BB'}$ analytical; ○, $\tau_{12}^{BB'}$ FDM; ——, $\tau_{12}^{BB'}$ analytical.

5.4. Design sensitivity analysis of energy density functions

The sensitivity results of the power transfer coefficient in Section 5.3 are obtained from the analytical expression in Appendix A. However, the sensitivity of the energy density can only be calculated by solving the sensitivity equation for the direct differentiation method, or by solving the adjoint equation for the adjoint variable method. In this section, the accuracy of the energy density sensitivity is compared with the sensitivity results obtained from FDM.

5.4.1. Parameter design sensitivity

Consider two plates that are placed at a right angle to each other from Section 5.3. In addition to having the same thickness and material properties as in Section 5.3, these plates also have a hysteresis-damping factor of $\eta = 0.01$. The dimension of each plate is $1\,\text{m} \times 1\,\text{m} \times 0.001\,\text{m}$, and 100 finite elements are used to approximate each plate. Fig. 14 shows the plate geometry with 200 finite elements. A unit power density with frequency 2.0 kHz is applied at node 61, which is the center of Plate 1. The objective is to estimate the variation of the energy density as a function of

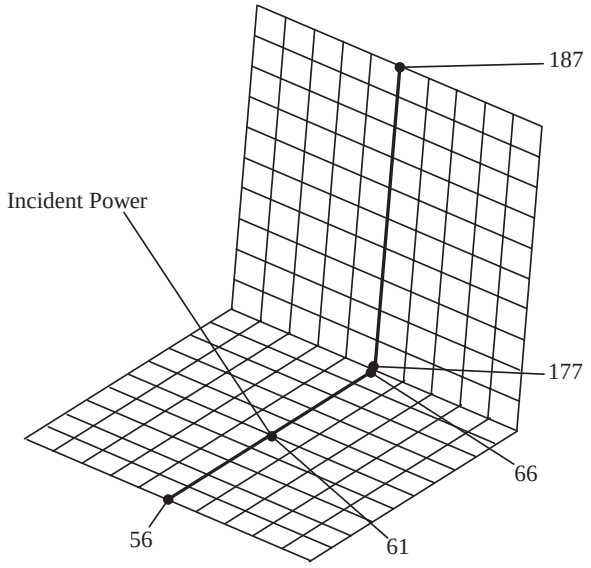

Fig. 14. Energy density distribution of two plates at a right angle.

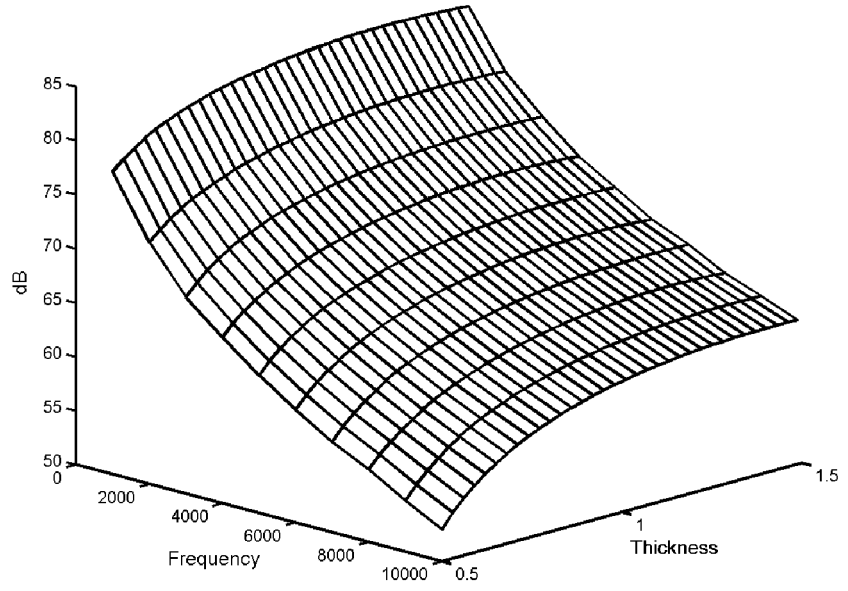

Fig. 15. Energy density as a function of frequency and plate thickness.

Plate 1's thickness by using the sensitivity calculation method. Before calculating the sensitivity information, the energy density distribution is plotted as a function of plate thickness and frequencies, as shown in Fig. 15. Even if the continuity of energy density function is not mathematically proven, Fig. 15 shows that the energy density function is a smooth function of plate thickness and frequency.

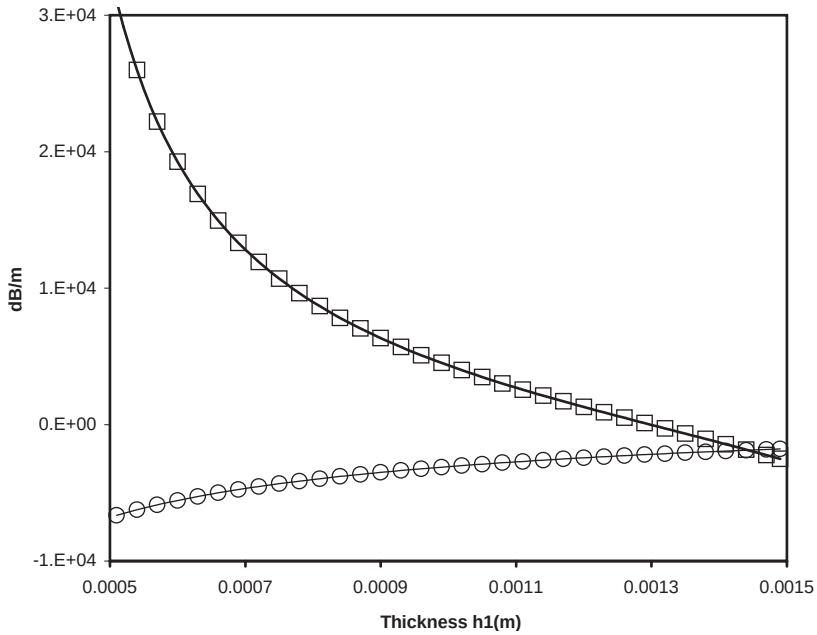

Fig. 16. Design sensitivity plot of the energy density with respect to the thickness design variable of plate 1 (2.0 kHz): ○, FDM P1; ——, DSA P1, □, FDM P2, ——, DSA P2.

Fig. 16 plots the sensitivity of energy density functions with respect to the thickness design of Plate 1. The location of point P1 is at the center of Plate 1, and the location P2 is at the center of Plate 2. "DSA P1" is the design sensitivity of energy density at P1 calculated from the proposed method, while "FDM P1" is the design sensitivity calculated using the FDM. A direct differentiation method is used to calculate the sensitivity of energy density functions. As the thickness of Plate 1 increases, more power is transferred to Plate 2. Thus, the energy density sensitivity decreases at point P1, while increasing at point P2. However, this pattern trails off as the thickness of Plate 1 approaches 1.5 mm. It is interesting that the energy density of point P2 starts to decrease when the thickness of Plate 1 becomes 1.3 mm. Thus, the maximum value of the energy density's sensitivity at point P2 can be expected at $h_1 = 1.3$ mm.

Table 2 compares the sensitivity results of energy densities for those nodes along the centerline of the plates (see Fig. 14). The same thickness of $h_1 = h_2 = 1.0$ mm is used for both plates. The energy density values are calculated from a frequency average that is over a one-third octave. The first and second columns denote the node number and nodal energy density (performance measure) in dB units, respectively. Performance changes are then denoted from the direct differentiation method (column 3), the adjoint variable method (column 4), and FDM (column 5). Column 5 is the ratio between columns 3 and 5, and column 6 is the ratio between columns 3 and 6. A small design perturbation of $\Delta h = 10^{-3}$ mm is used. The results from the two proposed methods are compared with the finite difference results in the ratio column (%). Excellent agreement is observed between the three methods. In fact, the sensitivity results from the direct differentiation and adjoint variable methods are the same up to the significant digits shown in the

Table 2
Comparison of sensitivity results obtained from the proposed and the finite difference methods ($\theta = 90^\circ$, $\omega = 2.0$ kHz)

Node	ψ	$\psi'\Delta\varepsilon$		$\Delta\psi$	$\Delta\psi/\psi'\Delta\varepsilon \times 100\%$	
		DDM	AVM		DDM	AVM
56	0.91237945E+2	0.40465093E-2	0.40465093E-2	0.40473102E-2	100.02	100.02
57	0.91404763E+2	0.24799215E-2	0.24799215E-2	0.24805766E-2	100.03	100.03
58	0.91908154E+2	−0.19791083E-2	−0.19791083E-2	−0.19788282E-2	99.99	99.99
59	0.92790054E+2	−0.89176064E-2	−0.89176064E-2	−0.89178111E-2	100.00	100.00
60	0.94039969E+2	−0.16996344E-1	−0.16996344E-1	−0.16996976E-1	100.00	100.00
61	0.97291986E+2	−0.30821719E-1	−0.30821719E-1	−0.30822884E-1	100.00	100.00
62	0.93991173E+2	−0.17396825E-1	−0.17396825E-1	−0.17397454E-1	100.00	100.00
63	0.92655044E+2	−0.97446228E-2	−0.97446228E-2	−0.97448706E-2	100.00	100.00
64	0.91644878E+2	−0.30619330E-2	−0.30619330E-2	−0.30618179E-2	100.00	100.00
65	0.90977247E+2	0.14228950E-2	0.14228950E-2	0.14231904E-2	100.02	100.02
66	0.90623021E+2	0.32388008E-2	0.32388008E-2	0.32389950E-2	100.01	100.01
177	0.83403422E+2	0.42493917E-1	0.42493917E-1	0.42499934E-1	100.01	100.01
178	0.82417283E+2	0.42846442E-1	0.42846442E-1	0.42852465E-1	100.01	100.01
179	0.81461217E+2	0.43069418E-1	0.43069418E-1	0.43075445E-1	100.01	100.01
180	0.80537757E+2	0.43210071E-1	0.43210071E-1	0.43216100E-1	100.01	100.01
181	0.79655424E+2	0.43298517E-1	0.43298517E-1	0.43304548E-1	100.01	100.01
182	0.78829343E+2	0.43353900E-1	0.43353900E-1	0.43359932E-1	100.01	100.01
183	0.78082023E+2	0.43388322E-1	0.43388322E-1	0.43394355E-1	100.01	100.01
184	0.77443423E+2	0.43409373E-1	0.43409373E-1	0.43415406E-1	100.01	100.01
185	0.76948922E+2	0.43421734E-1	0.43421734E-1	0.43427767E-1	100.01	100.01
186	0.76633956E+2	0.43428182E-1	0.43428182E-1	0.43434215E-1	100.01	100.01
187	0.76525562E+2	0.43430179E-1	0.43430179E-1	0.43436213E-1	100.01	100.01

table. Note that the energy density values of the two junction nodes 66 and 177 are different at about 7.2 dB, which confirms the discontinuity of energy density across the junction.

As a final example of parameter design sensitivity analysis, a hysteresis-damping factor is considered as a design variable. Fig. 17 compares the sensitivity of energy densities from the proposed method and the FDM when the damping factor is the design variable. The effect of the damping factor on the energy density function is always negative for Plate 2. However, such an effect gradually decreases, and shows saturation as the damping factor approaches to 0.1. The effect of the damping factor on Plate 1 is quite different from its effect on Plate 2. At the very small value of η (0.01–0.028), increasing the damping factor reduces the energy density at Plate 1. However, at a high value, the damping factor actually increases the energy density at Plate 1, and its effect is gradually reduced as the damping factor increases.

The energy density's dependence on the damping factor cannot be generalized because observations in this section depend on excitation frequency, material property, and plate dimensions. However, this example clearly shows that adding more damping material does not always guarantee a reduction in the noise level of structural components. In order to control the noise level, the effect of damping material must be fully understood in each component through design sensitivity analysis.

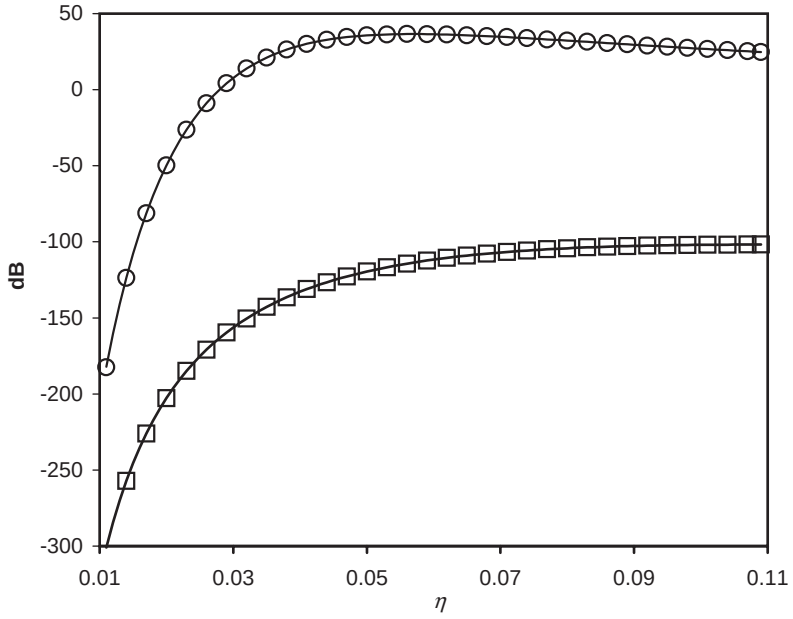

Fig. 17. Design sensitivity plot of the energy density with respect to the hysteresis-damping factor (2.0 kHz): ○, FDM P1; ——DSA P1; □, FDM P2; ——, DSA P2.

5.4.2. Shape design sensitivity

The same plate example used in Section 5.4.1 is now used to calculate energy density sensitivity with respect to the junction angle design variable. Fig. 18 illustrates the sensitivity of energy densities at the centers of Plates 1 and 2. This plot represents the change of energy density per unit radian angle change. Very high sensitivities are observed on Plate 2 near the junction angles 0° and 180°. However, the energy density value of Plate 1 is always greater than the energy density value of Plate 2.

The sensitivity results from the direct differentiation and adjoint variable methods are compared with the finite difference sensitivity results in Table 3. The energy density and its sensitivity are calculated when the junction angle is 90°. A small design perturbation of $\Delta\theta = 1^\circ$ is used for the FDM. At junction angle 90°, the sensitivity of Plate 1 (incident plate) is positive, while the sensitivity of Plate 2 (recipient plate) is negative. Thus, the energy of Plate 1 increases, while the energy of Plate 2 decreases as the junction angle increases. Sensitivity results from the direct differentiation and adjoint variable methods are again the same up to the significant digits shown in Table 3, and excellent agreement is observed between all three methods.

6. Conclusion

The design sensitivity formulation of the energy FEM is presented using the direct differentiation and adjoint variable methods. Material property, panel thickness, junction angle,

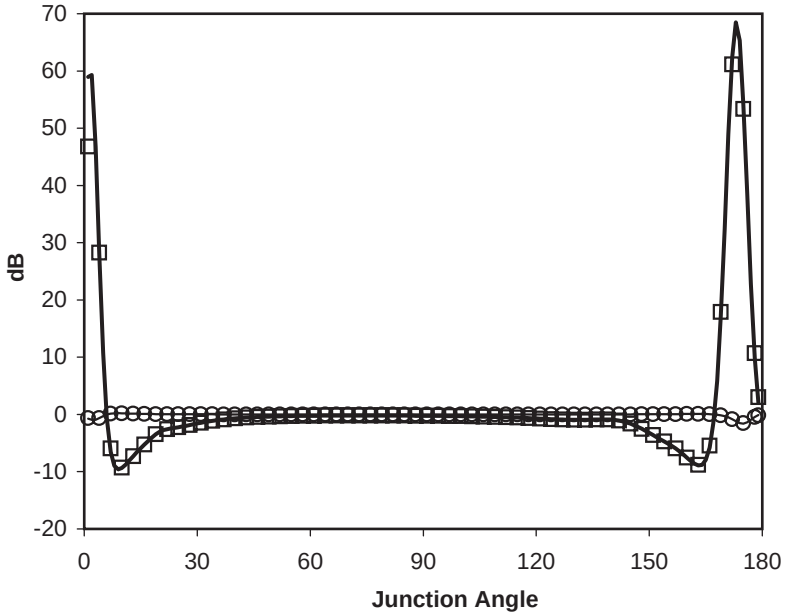

Fig. 18. Design sensitivity plot of the energy density with respect to the junction angle design variable ($\omega = 2.0$ kHz): ○, FDM P1; ——DSA P1; □, FDM P2; ——, DSA P2.

Table 3
Comparison of sensitivity results obtained from the proposed and the finite difference methods ($\theta = 90^\circ$, $\omega = 2.0$ kHz)

Node	ψ	$\psi'\Delta\theta$		$\Delta\psi$	$\Delta\psi/\psi'\Delta\theta \times 100\%$	
		DDM	AVM		DDM	AVM
56	0.91237945E+2	0.13120739E-3	0.13120739E-3	0.13124480E-3	100.03	100.03
57	0.91404763E+2	0.13120739E-3	0.13120739E-3	0.12949254E-3	100.03	100.03
58	0.91908154E+2	0.12396388E-3	0.12396388E-3	0.12399922E-3	100.03	100.03
59	0.92790054E+2	0.11339322E-3	0.11339322E-3	0.11342555E-3	100.03	100.03
60	0.94039969E+2	0.98517380E-4	0.98517380E-4	0.98545473E-4	100.03	100.03
61	0.97291986E+2	0.55350131E-4	0.55350131E-4	0.55365918E-4	100.03	100.03
62	0.93991173E+2	0.14324571E-3	0.14324571E-3	0.14328655E-3	100.03	100.03
63	0.92655044E+2	0.23895774E-3	0.23895774E-3	0.23902582E-3	100.03	100.03
64	0.91644878E+2	0.37350101E-3	0.37350101E-3	0.37360731E-3	100.03	100.03
65	0.90977247E+2	0.54398042E-3	0.54398042E-3	0.54413505E-3	100.03	
66	0.90623021E+2	0.74303209E-3	0.74303209E-3	0.74324297E-3	100.03	100.03
177	0.83403422E+2	−0.41517066E-2	−0.41517066E-2	−0.41528708E-2	100.03	100.03
178	0.82417283E+2	−0.41409977E-2	−0.41409977E-2	−0.41421588E-2	100.03	100.03
179	0.81461217E+2	−0.41342314E-2	−0.41342314E-2	−0.41353905E-2	100.03	100.03
180	0.80537757E+2	−0.41299652E-2	−0.41299652E-2	−0.41311231E-2	100.03	100.03
181	0.79655424E+2	−0.41272831E-2	−0.41272831E-2	−0.41284402E-2	100.03	100.03
182	0.78829343E+2	−0.41256038E-2	−0.41256038E-2	−0.41267604E-2	100.03	100.03
183	0.78082023E+2	−0.41245601E-2	−0.41245601E-2	−0.41257164E-2	100.03	100.03
184	0.77443423E+2	−0.41239219E-2	−0.41239219E-2	−0.41250779E-2	100.03	100.03
185	0.76948922E+2	−0.41235471E-2	−0.41235471E-2	−0.41247031E-2	100.03	100.03
186	0.76633956E+2	−0.41233516E-2	−0.41233516E-2	−0.41245075E-2	100.03	100.03
187	0.76525562E+2	−0.41232910E-2	−0.41232910E-2	−0.41244469E-2	100.03	100.03

and structural shape are taken into account as design variables, in addition to the hysteresis-damping factor. The continuum approach is used to derive the design sensitivity formulation of the structural component, while the discrete approach is used to obtain the design sensitivity of the junction matrix, which is required in the coupling of different components. The analytical expression of the power transfer coefficient is differentiated with respect to the design variables to obtain the power transfer coefficient sensitivity. The design sensitivity results calculated from the proposed method are compared with the finite difference sensitivity results with good agreement. The proposed design sensitivity calculation method is integrated into the design optimization process.

Acknowledgements

This research is supported by the Automotive Research Center that is sponsored by the US Army TARDEC under contract DAAE07-94-C-R094. We gratefully acknowledge this support.

Appendix A. Power transfer coefficient

In this section, the analytical methods for calculating the power-transfer coefficient τ_{ij} and its sensitivity with respect to panel thickness and junction angle are briefly summarized. The detailed procedure for calculating τ_{ij} can be found in [29]. In the plate structure, three types of incident wave can be considered: bending, in-plane, and shear waves. In this section, the formulation with the bending incident wave is developed. However, other types of waves can also developed using a similar approach.

A.1. Calculation of power transfer coefficients

Consider two or more plate structures connected at a junction. An N number of plates are connected at the junction. For convenience, Plate 1 has an incident wave, and Plates 2–N are recipient. Fig. 19 presents the simple case in which $N = 2$. In the derivation, index i represents the incident plate, while index j represents the recipient plate. A body-fixed local co-ordinate system $x_j - y_j - z_j$ is drawn for Plate j at the junction. The co-ordinate system fixed in Plate i is denoted by $x_g - y_g - z_g$. The objective is to calculate the power transfer coefficient with respect to an incident wave with angle ϕ, and then, to integrate it between $[0, \pi]$ ranges.

The power transfer coefficients are calculated by applying a unit power to the incident plate, and the reflected and transferred powers are calculated using the dynamic stiffness matrix method. Since transferred powers are proportional to the wave amplitude, the wave amplitude of the jth plate is first calculated as

$$\boldsymbol{\alpha}_j = \boldsymbol{G}_j^{-1} \boldsymbol{b}_j, \tag{A.1}$$

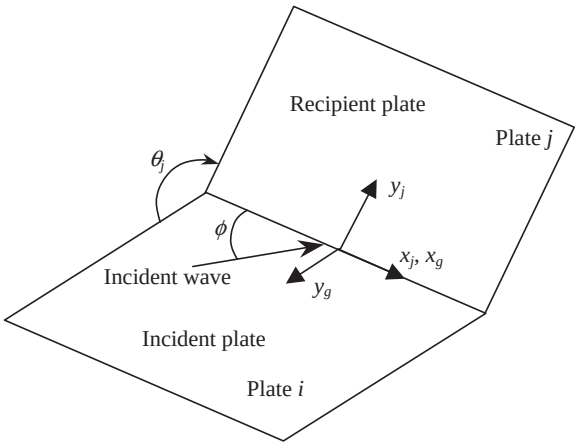

Fig. 19. Two infinite plates with a junction.

where $\boldsymbol{\alpha}_j^{\mathrm{T}} = [\alpha_L, \alpha_S, \alpha_{B1}, \alpha_{B2}]_j$ is the wave amplitude of transferred waves to the jth plate, $\boldsymbol{b}_j^{\mathrm{T}} = [u_e, v_e, w_e, \theta_e]_j$ is the edge displacement in the body-fixed local co-ordinate system, and

$$\boldsymbol{G}_j = \begin{bmatrix} k & \mathrm{j}\mu_S & 0 & 0 \\ \mathrm{j}\mu_L & -k & 0 & 0 \\ 0 & 0 & 1 & 1 \\ 0 & 0 & \mu_{B1} & \mu_{B2} \end{bmatrix}_j. \tag{A.2}$$

When k_B, k_L, and k_S are the wave numbers corresponding to bending, longitudinal, and shear waves in Eqs. (A.10)–(A.12), respectively, μ_{B1}, μ_{B2}, μ_L, and μ_S are the negative roots of the following equation:

$$\begin{aligned} \mu_{B1,2}^2 &= k^2 \pm k_B^2, \\ \mu_L^2 &= k^2 - k_L^2, \\ \mu_S^2 &= k^2 - k_S^2. \end{aligned} \tag{A.3}$$

Since the edge displacement vector $\boldsymbol{b}_j$ is represented in the local coordinate system $x_j - y_j - z_j$, it must be transformed into the global coordinate system by

$$\boldsymbol{b}_j = \boldsymbol{R}_j^{\mathrm{T}} \boldsymbol{a}, \tag{A.4}$$

where $\boldsymbol{a}^{\mathrm{T}} = [u_e, v_e, w_e, \theta_e]_g$ is the edge displacement vector in the global co-ordinate system and

$$\boldsymbol{R}_j = \begin{bmatrix} 1 & 0 & 0 & 0 \\ 0 & \cos\theta_j & -\sin\theta_j & 0 \\ 0 & \sin\theta_j & \cos\theta_j & 0 \\ 0 & 0 & 0 & 1 \end{bmatrix}, \tag{A.5}$$

is the co-ordinate transformation matrix. Note that the x_j-axis is parallel to the junction, as shown in Fig. 19. From Eqs. (A.1) and (A.4), the wave amplitude can be expressed in terms of global edge displacement as

$$\boldsymbol{\alpha}_j = \boldsymbol{G}_j^{-1}\boldsymbol{R}_j^{\mathrm{T}}\boldsymbol{a}. \tag{A.6}$$

Thus, the wave amplitude can be calculated from the edge displacement, which can be calculated from the dynamic stiffness method.

The edge displacement can be found by considering the equilibrium of the structure under the force caused by the unit incident wave. The force equilibrium equation can be written as

$$\left\{\sum_{j=1}^{N}\boldsymbol{R}_j\boldsymbol{K}_j\boldsymbol{R}_j^{\mathrm{T}}\right\}\boldsymbol{a} \equiv \boldsymbol{C}\boldsymbol{a} = \boldsymbol{R}_i\boldsymbol{f}_i, \tag{A.7}$$

where $\boldsymbol{K}_j$ is the dynamic stiffness matrix, $\boldsymbol{f}_i$ is the edge force caused by the incident wave, and N is the number of plates connected at the junction. The expressions of $\boldsymbol{K}_j$ and $\boldsymbol{f}_i$ are provided by Langley and Heron [29]. By solving Eq. (A.7) for $\boldsymbol{a}$ and substituting the result into Eq. (A.6), the wave amplitude vector are obtained as

$$\boldsymbol{\alpha}_j = \boldsymbol{G}_j^{-1}\boldsymbol{R}_j^{\mathrm{T}}\boldsymbol{C}^{-1}\boldsymbol{R}_i\boldsymbol{f}_i. \tag{A.8}$$

After calculating the wave amplitude $\boldsymbol{\alpha}_j$, the power transfer coefficients can be calculated through the integration over the incident wave angle as

$$\begin{aligned}
\tau_{ij}^{BB} &= \frac{1}{2}\int_0^{\pi}\frac{\rho_j}{\rho_i}\frac{h_j}{h_i}\frac{k_{Bi}}{k_{Bj}}|\alpha_{B2j}|^2\sqrt{1-(k/k_{Bj})^2}\,\mathrm{d}\phi,\\
\tau_{ij}^{BL} &= \frac{1}{4}\int_0^{\pi}\frac{\rho_j}{\rho_i}\frac{h_j}{h_i}k_{Bi}k_{Lj}|\alpha_{Lj}|^2\sqrt{1-(k/k_{Lj})^2}\,\mathrm{d}\phi,\\
\tau_{ij}^{BS} &= \frac{1}{4}\int_0^{\pi}\frac{\rho_j}{\rho_i}\frac{h_j}{h_i}k_{Bi}k_{Sj}|\alpha_{Sj}|^2\sqrt{1-(k/k_{Sj})^2}\,\mathrm{d}\phi,
\end{aligned} \tag{A.9}$$

where ρ is the material density, h is the plate thickness, and

$$k_{Bj} = \left(\frac{12\rho_j\omega^2(1-\nu_j^2)}{E_j h_j^2}\right)^{1/4}, \tag{A.10}$$

$$k_{Lj} = \left(\frac{\rho_j\omega^2(1-\nu_j^2)}{E_j}\right)^{1/2}, \tag{A.11}$$

$$k_{Sj} = \left(\frac{2\rho_j\omega^2(1+\nu_j)}{E_j}\right)^{1/2} \tag{A.12}$$

and $k = k_{Bi}\cos\phi$ when the incident wave is the bending wave. As can be seen from Eqs. (A.9)–(A.12), the power transfer coefficients are a function of material properties, plate thickness, and junction angle, which are design variables.

A.2. Sensitivity of power transfer coefficients with respect to junction angle

Let junction angles θ_j of Plate j be measured with respect to the incident plate. When the junction angle is the design variable, only the wave amplitude in Eq. (A.9) depends on the design. Thus, the sensitivity of the power transfer coefficients can be written as

$$\begin{aligned}
\tau_{ij}^{BB'} &= \frac{1}{2}\int_0^{\pi}\frac{\rho_j}{\rho_i}\frac{h_j}{h_i}\frac{k_{Bi}}{k_{Bj}}\frac{\partial\left|\alpha_{B2j}\right|^2}{\partial\theta_j}\sqrt{1-(k/k_{Bj})^2}\,\mathrm{d}\phi\delta\theta_j,\\
\tau_{ij}^{BL'} &= \frac{1}{4}\int_0^{\pi}\frac{\rho_j}{\rho_i}\frac{h_j}{h_i}k_{Bi}k_{Lj}\frac{\partial\left|\alpha_{Lj}\right|^2}{\partial\theta_j}\sqrt{1-(k/k_{Lj})^2}\,\mathrm{d}\phi\delta\theta_j,\\
\tau_{ij}^{BS'} &= \frac{1}{4}\int_0^{\pi}\frac{\rho_j}{\rho_i}\frac{h_j}{h_i}k_{Bi}k_{Sj}\frac{\partial\left|\alpha_{Sj}\right|^2}{\partial\theta_j}\sqrt{1-(k/k_{Sj})^2}\,\mathrm{d}\phi\delta\theta_j.
\end{aligned} \tag{A.13}$$

The derivative of the wave amplitude with respect to the junction angle can be obtained by differentiating Eq. (A.8) as

$$\frac{\partial\boldsymbol{\alpha}_j}{\partial\theta_j} = \boldsymbol{G}_j^{-1}\frac{\partial\boldsymbol{R}_j^{\mathrm{T}}}{\partial\theta_j}\boldsymbol{C}^{-1}\boldsymbol{R}_i\boldsymbol{f}_i - \boldsymbol{G}_j^{-1}\boldsymbol{R}_j^{\mathrm{T}}\boldsymbol{C}^{-1}\frac{\partial\boldsymbol{C}}{\partial\theta_j}\boldsymbol{C}^{-1}\boldsymbol{R}_i\boldsymbol{f}_i. \tag{A.14}$$

Note that $\boldsymbol{R}_i$ is independent of the junction angle because the angle of the incident plate is the reference. From the definition in Eq. (A.7), the derivative of matrix $\boldsymbol{C}$ can be evaluated as

$$\frac{\partial\boldsymbol{C}}{\partial\theta_j} = \frac{\partial\boldsymbol{R}_j}{\partial\theta_j}\boldsymbol{K}_j\boldsymbol{R}_j^{\mathrm{T}} + \boldsymbol{R}_j\boldsymbol{K}_j\frac{\partial\boldsymbol{R}_j^{\mathrm{T}}}{\partial\theta_j}. \tag{A.15}$$

Since the angle of Plate j changes, other recipient plates are independent of θ_j. Thus, the summation used in Eq. (A.7) is not necessary.

A.3. Sensitivity of power transfer coefficients with respect to thickness

The sensitivity of power transfer coefficients with respect to the thickness design variable is more complicated than the junction angle design variable. In this section, the thickness of recipient plate j is considered as a design variable. A similar approach can be applied to the thickness of the incident wave with algebraic messiness.

In the expression of wave amplitude, the matrices $\boldsymbol{G}_j$ and $\boldsymbol{C}$ depend on the thickness h_j. Thus, the chain rule of differentiation yields

$$\frac{\partial\boldsymbol{\alpha}_j}{\partial h_j} = -\boldsymbol{G}_j^{-1}\frac{\partial\boldsymbol{G}_j}{\partial h_j}\boldsymbol{G}_j^{-1}\boldsymbol{R}_j^{\mathrm{T}}\boldsymbol{C}^{-1}\boldsymbol{R}_i\boldsymbol{f}_i - \boldsymbol{G}_j^{-1}\boldsymbol{R}_j^{\mathrm{T}}\boldsymbol{C}^{-1}\frac{\partial\mathbf{C}}{\partial h_j}\boldsymbol{C}^{-1}\boldsymbol{R}_i\boldsymbol{f}, \tag{A.16}$$

where

$$\frac{\partial\boldsymbol{C}}{\partial h_j} = \boldsymbol{R}_j\frac{\partial\boldsymbol{K}_j}{\partial h_j}\boldsymbol{R}_j^{\mathrm{T}}, \tag{A.17}$$

$$\frac{\partial \boldsymbol{G}_j}{\partial h_j} = \begin{bmatrix} 0 & 0 & 0 & 0 \\ 0 & 0 & 0 & 0 \\ 0 & 0 & 0 & 0 \\ 0 & 0 & \dfrac{k_{Bj}}{\mu_{B1j}} \dfrac{\partial k_{Bj}}{\partial h_j} & -\dfrac{k_{Bj}}{\mu_{B2j}} \dfrac{\partial k_{Bj}}{\partial h_j} \end{bmatrix}, \tag{A.18}$$

where $\partial k_{Bj}/\partial h_j$ can be calculated from the expression in Eq. (A.10). In the derivation of Eq. (A.18), the property $\partial k/\partial h_j = \partial \mu_{Lj}/\partial h_j = \partial \mu_{Sj}/\partial h_j = 0$ is used.

After calculating $\partial \boldsymbol{\alpha}/\partial h_j$ in Eq. (A.16), the sensitivity of τ_{ij} can be calculated by differentiating Eq. (A.9), which simply involves using the chain rule of differentiation.

References

[1] Z.-D. Ma, I. Hagiwara, Sensitivity analysis—method for coupled acoustic–structural systems Part 1: modal sensitivities, Part 2: direct frequency–response and its sensitivities, American Institute of Aeronautics and Astronautics Journal 29 (1991) 1787–1801.

[2] S. Wang, K.K. Choi, H. Kularni, Acoustical optimization of vehicle passenger space, 1994, SAE Paper No. 941071.

[3] R.R. Salagame, A.D. Belegundu, G.H. Koopman, Analytical sensitivity of acoustic power radiated from pates, Journal of Vibration and Acoustics 117 (1995) 43–48.

[4] K.K. Choi, I. Shim, S. Wang, Design sensitivity analysis of structure–induced noise and vibration, Journal of Vibration and Acoustics 119 (1997) 173–179.

[5] F. Scarpa, Parametric sensitivity analysis of coupled acoustic–structural systems, Journal of Vibration and Acoustics 122 (2000) 109–115.

[6] J.H. Kane, S. Mauo, G.C. Everstine, Aboundary element formulation for acoustic shape sensitivity analysis, Journal of the Acoustical Society of America 90 (1991) 561–573.

[7] D.C. Smith, R.J. Bernhard, Computation of acoustic shape design sensitivity using a boundary element method, Journal of Vibration and Acoustics 114 (1992) 127–132.

[8] K.A. Cunefare, G.H. Koopman, Acoustic design sensitivity for structural radiators, Journal of Vibration and Acoustics 114 (1992) 179–186.

[9] T. Matsumoto, M. Tanaka, Y. Yamada, Design sensitivity analysis of steady–state acoustic problems using boundary integral equation formulation, JSME International Journal Series C 38 (1995) 9–16.

[10] B.U. Koo, Shape design sensitivity analysis of acoustic problems using a boundary element method, Computers and Structures 65 (1997) 713–719.

[11] N.H. Kim, J. Dong, K.K. Choi, N. Vlahopoulos, Z.-D. Ma, M. Castanier, C. Pierre, Design sensitivity analysis for sequential structural–acoustic problems, Journal of Sound and Vibration 263 (2003) 569–591.

[12] D.J. Nefske, J.A. Wolf, L.J. Howell, Structural–acoustic finite element analysis of the automobile passenger compartment: a review of current practice, Journal of Sound and Vibration 80 (1982) 247–266.

[13] R. Lyon, Statistical Energy Analysis of Dynamical Systems: Theory and Application, The MIT Press, Cambridge, MA, 1975.

[14] F.J. Fahy, Statistical energy analysis: a critical review, The Shock and Vibration Digest 6 (1) (1974) 14–33.

[15] R. Lyon, R.G. DeJong, Theory and Application of Statistical Energy Analysis, 2nd Edition, Butterworth-Heinemann, Boston, MA, 1995.

[16] L.K.H. Lu, Optimum damping selection by statistical energy analysis, Statistical Energy Analysis, Winter Annual Meeting, Boston, MA, 1995, pp. 9–14

[17] S.A. Rybak, Waves in plate containing random inhomogeneities, Soviet Physics and Acoustics 17 (1972) 345–349.

[18] V.D. Belov, S.A. Rybak, B.D. Tartakovskii, Propagation of vibrational energy in absorbing structures, Soviet Physics and Acoustics 23 (1977) 115–119.
[19] D.J. Nefske, S.H. Sung, Power flow finite-element analysis of dynamic-systems—basic theory and application to beams, Journal of Vibration, Acoustics, Stress, and Reliability in Design 111 (1989) 94–100.
[20] J. Wohlever, R.J. Bernhard, Mechanical energy flow models of rods and beams, Journal of Sound and Vibration 153 (1992) 1–19.
[21] O.M. Bouthier, R.J. Bernhard, Models of space-averaged energetics of plates, American Institute of Aeronautics and Astronautics Journal 30 (1992) 616–623.
[22] O.M. Bouthier, R.J. Bernhard, Simple–models of the energetics of transversely vibrating plates, Journal of Sound and Vibration 182 (1995) 149–166.
[23] P. Cho, R.J. Bernhard, Energy flow analysis of coupled beams, Journal of Sound and Vibration 211 (1998) 593–605.
[24] N. Vlahopoulos, L.O. Garza-Rios, C. Mollo, Numerical implementation, validation, and marine applications of an energy finite element formulation, Journal of Ship Research 43 (1999) 143–156.
[25] F. Bitsie, R.J. Bernhard, Sensitivity calculations for structural–acoustic EFEM predictions, Noise Control Engineering Journal 46 (1998) 91–96.
[26] R.J. Bernhard, J.E. Huff, Structural–acoustic design at high frequency using the energy finite element method, Journal of Vibration and Acoustics 121 (1999) 295–301.
[27] G.A. Borlase, N. Vlahopoulos, An energy finite element optimization process for reducing high-frequency vibration in large-scale structures, Finite Elements in Analysis and Design 36 (2000) 51–67.
[28] K.K. Choi, E.J. Haug, Shape design sensitivity analysis of elastic structures, Journal of Structural Mechanics 11 (1983) 231–269.
[29] R.S. Langley, K.H. Heron, Elastic wave transmission through plate/beam junctions, Journal of Vibration and Acoustics 143 (1990) 241–253.
[30] K. De Langhe, P. Sas, D. Vandepitte, The use of wave-absorbing elements for the evaluation of transmission characteristics of beam junctions, Journal of Vibration and Acoustics 119 (1997) 293–303.
[31] N. Vlahopoulos, X. Zhao, T. Allen, An approach for evaluating power transfer coefficients for spot-welded joints in an energy finite element formulation, Journal of Sound and Vibration 220 (1999) 135–154.
[32] L. Cremer, L. Heckel, E.E. Ungar, Structure-Borne Sound: Structural Vibrations and Sound Radiational Audio Frequencies, 2nd Edition, Springer, Berlin, 1988.
[33] P.E. Cho, Energy flow analysis of coupled structures, Ph.D. Thesis, Purdue University, West Lafayette, IN, 1993.
[34] M. Gelfand, S.V. Fomin, Calculus of Variations, Prentice-Hall, Englewood Cliffs, NJ, 1963.